

Article

# Mineralogical, Rock-Magnetic and Palaeomagnetic Properties of Metadolerites from Central Western Svalbard

Mariusz Burzyński <sup>1,\*</sup>, Krzysztof Michalski <sup>1</sup>, Geoffrey Manby <sup>2</sup>  and Krzysztof Nejbart <sup>3</sup>

<sup>1</sup> Institute of Geophysics Polish Academy of Sciences, ul. Księcia Janusza 64, 01-452 Warszawa, Poland; krzysztof.michalski@igf.edu.pl

<sup>2</sup> Natural History Museum, London, Cromwell Road, London SW7 5BD, UK; g.m.manby@btinternet.com

<sup>3</sup> Department of Geology, University of Warsaw, ul. Żwirki i Wigury 93, 02-089 Warszawa, Poland; knejbart@uw.edu.pl

\* Correspondence: mburzynski@igf.edu.pl; Tel.: +48-501-267-903

Received: 28 May 2018; Accepted: 26 June 2018; Published: 29 June 2018



**Abstract:** A combination of mineralogical, rock-magnetic and palaeomagnetic methods were employed in an attempt to shed a new light on the tectonism and paleogeography of Central Western Svalbard. The focus is on six metadolerite sites from the metamorphic Proterozoic–Lower Palaeozoic complex of south-western Oscar II Land (Western Spitsbergen). The primary mineral compositions of the metadolerites were strongly remineralized during Caledonian (*sensu lato*) greenschist-facies metamorphism although some younger tectonothermal modification is also apparent from the rock-magnetic studies. Rock-magnetic experiments supported by thin-section mineral identification and separation of Fe-containing fractions indicate that the main ferromagnetic carriers of the Natural Remanent Magnetization are represented by low-coercivity pyrrhotite and magnetite/maghemite. The investigated metadolerites are characterized by complex pattern of magnetization. The low-temperature palaeomagnetic components which demagnetized up to 250 °C, are characterized by high inclinations (~70–80°) potentially representing Mesozoic–Cenozoic remagnetization. The most stable middle-high temperature directions which demagnetized from 250 °C, were obtained from only two of six sites. Two Virtual Geomagnetic Poles calculated from two of the middle-high temperature site means do not correlate with the Laurussia reference path for syn- to post-Caledonian time. Two possible explanations of observed inconsistency are discussed. These are a modification of the Oscar II Land Caledonian basement geometry by listric faulting and/or tectonic rotations related to Daudmannsdalen–Protectorbreen high-strain (shear) zone. The results presented here suggest that post-Caledonian tectonic modification of the palaeomagnetic directions may be more a widespread feature of Western Svalbard.

**Keywords:** magnetic mineralogy; rock-magnetic experiments; palaeomagnetism; Arctic; Western Spitsbergen

## 1. Introduction

This contribution presents the results of combined palaeomagnetic, rock-magnetic and mineralogical analysis of six metadolerite sites from the Proterozoic–Lower Palaeozoic (?) metamorphic complex of the Daudmannsdalen–Daudmannsøyra–Protectorbreen area of south-western Oscar II Land (OII) (Figure 1).

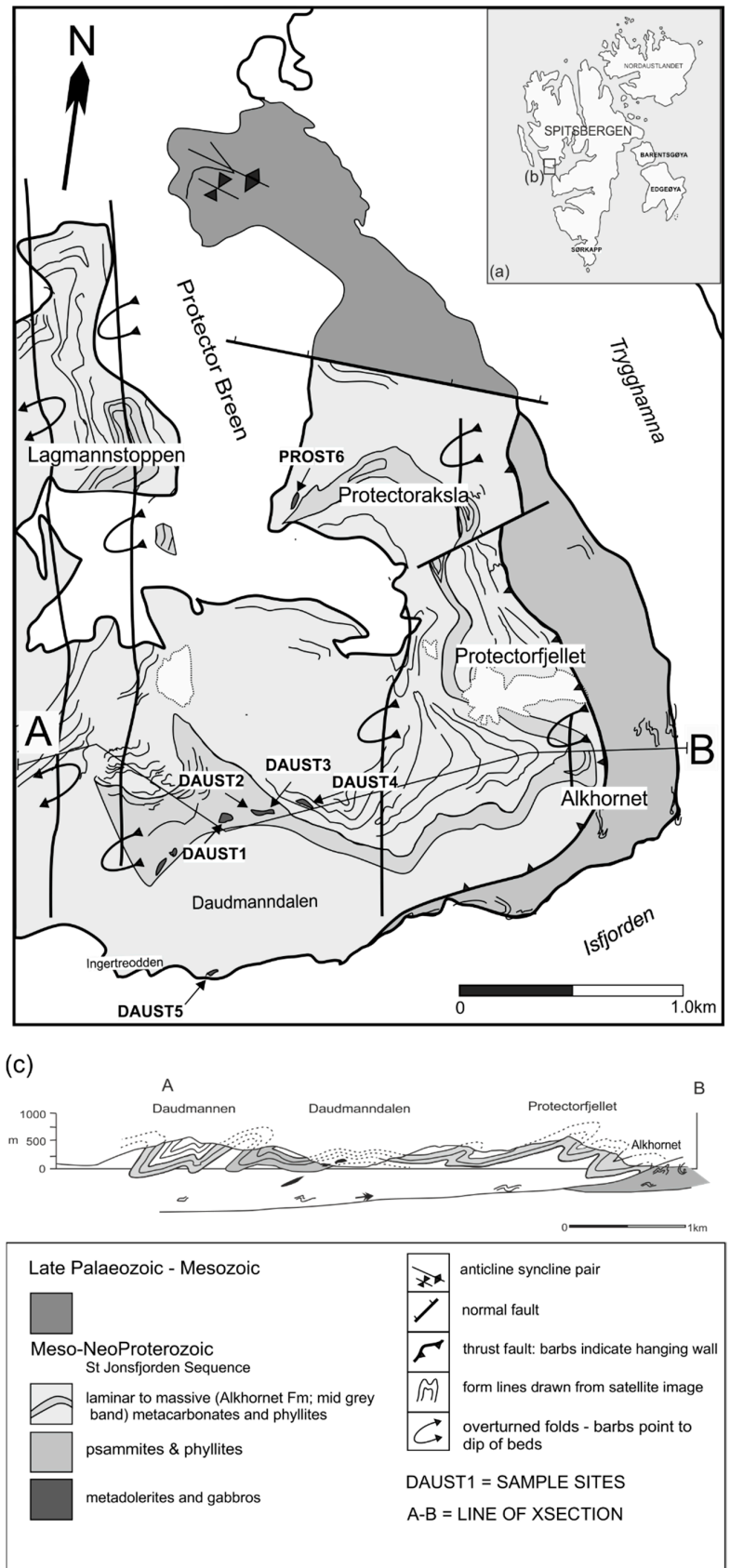


**Figure 1.** (a) Locations of palaeomagnetic sites are given; (b) Geological sketch map of SW Oscar II Land; (c) Geological cross-section (A–B) across Daudmannen to Alkhornet.

According to Harland and Wright [1] the Caledonian basement of Svalbard can be divided into an Eastern, a Central and a Western Terrane, which were amalgamated from disparate locations along the Eastern and NE Greenland margins in Late Devonian time. The area of SW Oscar II Land (OIIL) investigated here belongs to the Western Svalbard Terrane [1].

An alternative view is proposed, for example, by Gee [2] and Gee and Page [3] who questioned the fault boundaries between Caledonian Terranes proposed by Harland and Wright [1] and redefined the division of Svalbard Caledonian basement into Northeastern (NEBP), Northwestern (NWBP) and Southwestern (SWBP) Basement Provinces. The latter division was accepted also by the other authors (e.g., [4–9]) and adopted in the Geoscience Atlas of Svalbard [10]. According to that classification OIIL area is a part of the Southwestern Basement Province (SWBP).

A number of publications suggests a possible affinity of Western Spitsbergen Proterozoic and L. Palaeozoic basement with Pearya or North Greenland (Laurentia; e.g., [4,5,7]). It is worth noting, however, that other authors [11], from a comparative study of detrital zircon populations in the Caledonian rocks of the St Jonsfjorden area and those of other Arctic Margins, have argued that the Western and Central Terranes *sensu* Harland and Wright [1] have similar histories to and a greater affinity with Northern Baltica. Michalski et al. [12] have questioned, from palaeomagnetic and isotopic data, the timing of the amalgamation of Svalbard [1] suggesting that the Eastern and Central Caledonian Svalbard Terranes *sensu* Harland and Wright [1] had already docked by Late Silurian time. Although several palaeomagnetic attempts have been undertaken to establish the pre-Caledonian palaeogeographic position of the pre-Late Devonian location of Western Svalbard [13,14], it remains unresolved.

This contribution follows on from previous studies of the metabasites by the authors in the St. Jonsfjorden, Venernbreen, Kinnefjellet, Ommafjellet areas of Western OIIL [14,15]. The metadolerite host rocks of western OIIL have been found, from in situ  $^{40}\text{Ar}/^{39}\text{Ar}$  data using a 1059 nm CSI fibre laser and MAP215-50 mass spectrometer, to have been subjected to three thermal events in the 426–380 Ma (Caledonian (*sensu lato*) metamorphism?), the 377–326 Ma and the ca. 300 Ma intervals. The two younger resetting ages could be related to the Late Palaeozoic rift-controlled extensional movements in the Barents Shelf as was suggested by Michalski et al. [14]. The 377–326 Ma overprint can be also correlated with Devonian–Carboniferous Svalbardian/Ellesmerian events [8,9,16–18]. All of the listed events could potentially have reset and/or overprinted the palaeomagnetic record. While the pre-metamorphic palaeomagnetic record of the metadolerites of western OIIL can, potentially, survive the Caledonian greenschist-facies metamorphism the rock-magnetic and mineralogical data reported by Michalski et al. [14] and Burzyński et al. [15] demonstrate that there are no relicts of any pre-Caledonian ferromagnetic carriers. Several palaeogeographic and tectonic models have been tested to explain inconsistency of the calculated palaeopoles with reference to the Apparent Polar Wander Path of Laurussia [14]. From palaeomagnetic and isotopic data it was postulated that listric normal faulting related to, for example, the opening of the North Atlantic, played an important role in the modification of the western OIIL Caledonian basement geometry [14].

The aim here is to determine of the pattern and origin of the Natural Remanent Magnetization (NRM) in the six newly investigated metadolerite sites within SW OIIL. Thermal and Alternating Field (AF) demagnetization technics were applied to define precisely the NRM components. While surviving pre-Caledonian palaeomagnetic directions would be needed to establish the Proterozoic–L. Palaeozoic palaeogeographical framework of the Svalbard—Greenland area secondary palaeomagnetic components can be used to check the extent to which subsequent contractional and extensional events have modified the geometry of the Caledonian metamorphic basement of Svalbard. Integrated rock-magnetic and mineralogical (optical/SEM/BSE/EPMA) investigations were undertaken to define precisely the origin of ferromagnetic minerals and check the possible preservation of any primary palaeomagnetic signal carriers. To increase the resolution of the results some of the rock-magnetic and mineralogical analyses were carried out on ferromagnetic separates. Additional analyses of the anisotropy of magnetic susceptibility (AMS: Appendix A) were conducted to better understand the

tectonic structure of investigated rocks and to assess the influence that any tectonic events may have had on palaeomagnetic record.

## 2. Geological Setting

Western Svalbard is generally considered to record the effects of multiphase magmatic, deformational and metamorphic episodes. The oldest examples of magmatism are of Stenian–Ectasian age and younger Tonian age ([8] and references therein) and were found mainly in Wedel Jarlsberg Land, SW Spitsbergen (Western Terrane/SWBP). Those rocks and associated metasedimentary successions were affected by Late Neoproterozoic Torellian metamorphism [19–21]. Torrellian deformations also affected two Early and Late Neoproterozoic metasedimentary succession from northern Wedel-Jarlsberg Land causing a regional-scale angular unconformity [22,23]. In those Neoproterozoic metasediments and others occurring across western Spitsbergen a further magmatic episode has been reported as a mafic dyke swarm and their extrusive equivalents (e.g., [14,15,24,25]). All those rocks were folded and affected by greenschist facies metamorphism during Caledonian (*sensu lato*) orogeny (for the numerous relevant references, see for example, [10,26]). Additionally, in western Spitsbergen there are several examples of high-pressure rocks related to subduction metamorphism [5,7,27]. The metabasic rocks described in this contribution may also have been subjected to Late Devonian–Early Carboniferous (Ellesmerian?) deformation, which was overprinted in Late Cretaceous–Palaeogene time by NE–E directed Eurekan folding and thrust faulting (see [9,10,17,26,28,29]). As a result of such complex tectonothermal history, there is a lack of coherence in the literature regarding the age and order of the pre-Caledonian stratigraphic succession of Oscar II Land (cf. [26,30–34]). Most of these accounts are based on the results of either regional reconnaissance or more in-depth localized fieldwork. As a result, there is also little consensus regarding the structural framework of the study area. For example, the 1:100,000 Geological Map of Svalbard (Isfjorden, Sheet B9G, [35]) interprets the pre-Caledonian St Jonsfjorden Sequence, which dominates the present study area, to be of Middle Proterozoic age. Harland [26], although providing no structural explanation in this tectonically complex area, argues that the whole of the St Jonsfjorden Group is of Vendian (early Varanger) age. Ohta et al. [35] indicates that, in the present study area, the repetition of the phyllite (unit 29) and the carbonate rocks (unit 28, or the Alkhornet Group of Harland [26]) has been imposed by thrust faulting. Field observations (e.g., Figure 2) and examination of the satellite images available from the NPI Kart over Svalbard website provide evidence for some of the repetition to be the result of large scale folding. These folds are characterized by N–S trending and plunging axial traces (Figure 1c) with shallow, west dipping axial surfaces. The metacarbonates forming the prominent buttress of Alkhornet, for example, constitutes an almost flat lying westward closing fold. A further the kilometric scale, near isoclinal, westward closing fold core can be traced across the Protectorfjellet to Protectoraksla ridge system (Figure 1b,c) and could account for the duplication of the phyllite-carbonate sequence [35]. A small ENE–WSW trending normal fault displaces the fold between the Protectorfjellet and Protectoraksla peaks down to the north. A similar pair of N–S trending large scale folds can be traced southwards across Lagmannstoppen ridges. The easternmost, west closing (synformal?) member, of this fold pair occupies the eastern slopes Lagmannstoppen and crosses Daudmannsbreen running southwards to the mountain front west of Daudmannsdalen (Figure 1c). Immediately west of this fold on the north–eastern slopes of Lagmannstoppen lies a further antiformal, east closing fold. The steep eastern and shallow western limb of this fold in particular suggests an eastward tectonic transport direction for this structure.

A further feature worthy of note is that the mountain ridges/fronts are cut by NNW trending families of predominantly west dipping fractures and small-scale faults. Other less common east dipping fractures and faults are apparent accommodating small rotations of the strata between the two sets of faults.

The investigated area is close to the proposed strike-slip, continent margin-parallel lineament extending from Svartfjella to Eidembukta to Daudmannsodden (the SEDL of Maher et al. [36]).

Tessensohn et al. [37], however, found no convincing evidence to confirm any such motion along the proposed SEDL lineament.

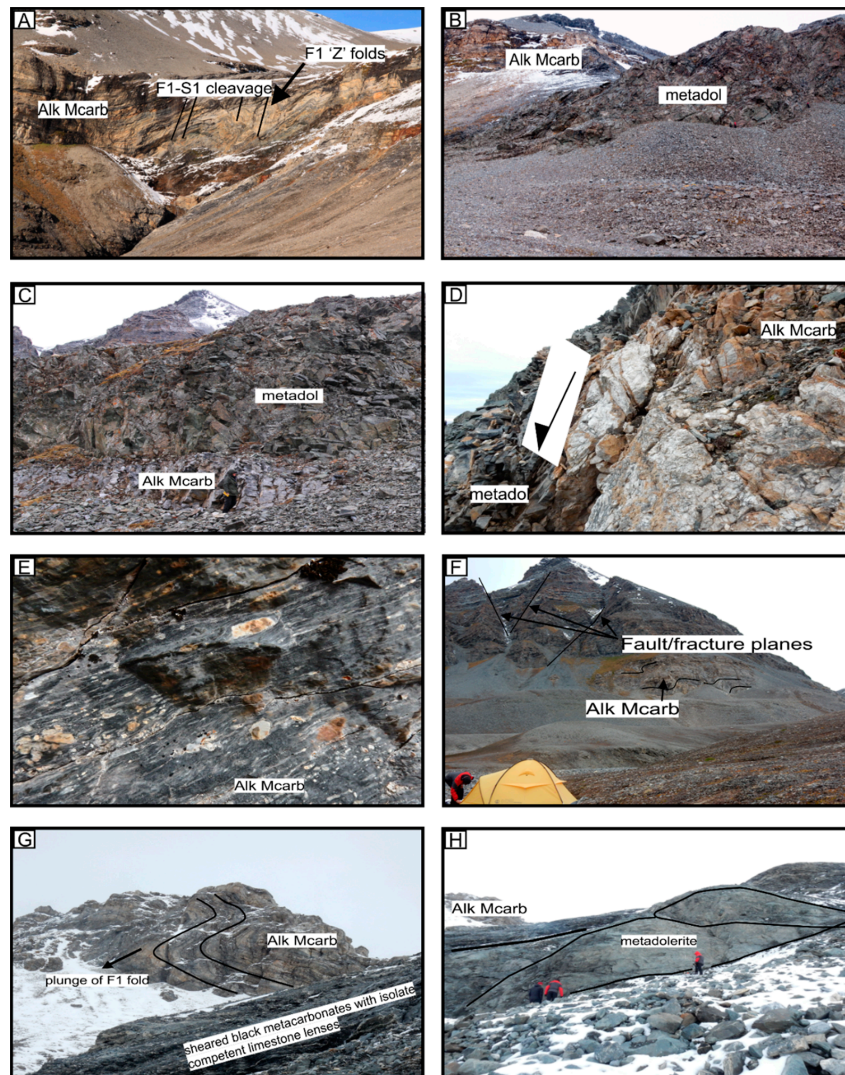


**Figure 2.** (A) Eastern flank of Daudmannsdalen showing F1 ‘z’ folds and S1 cleavage developed in the Alkhornet metacarbonates (Alk Mcarb) (B) Metadolerite (metadol) boudin at site DAUST2. intruded into Alkhornet metacarbonates. Boudin is cut by veral shear surfaces (C) Contact between Alkhornet metacarbonates and metadolerites. Bedding in the metacarbonates dips shallowly NW but steep fractures cut across the contact zone. Site DAUST3 (D) Metadolerite/carbonate contact zone with downfaulted dolerite (arrowed). Note the brecciation of the calcite veining in the late W dipping fault zone. Site DAUST3 (E) Metacarbonates just beneath the contact with the metadolerites are sheared with a top to the east shear sense. Site DAUST3 (F) Daudmannsdalen west flank minor ‘S’ geometry F1 folds indicating the upper limb of a west closing larger scale fold. Also note the west dipping and antithetic east dipping fault/fracture planes (arrowed). (G) Field view of PROST6 site the upper part of the photograph shows a N plunging ‘z’ fold in the Alkhornet metacarbonates. The underlying dark grey to black metacarbonates in the lower right of the view are the host rocks for the metadolerite shown in (H). The former, which are highly sheared, wrap around the metadolerite boudin and include, lenses of more competent limestones that represent isolated fold limbs. (H) Field view of PROST6 metadolerite sample site. Internally, the boudin is divided into smaller lenses (marked) that are cut by fracture/small scale fault planes. Above the boudin, top right, shows transitional facies from dark grey to Alkhornet-type metacarbonates.

The metadolerites targeted in this study are intruded into the thickly bedded Alkhornet metacarbonates in the Daudmannsdalen area (Figure 1b). On the western valley side of Daudmannsdalen the host metacarbonates exhibit N plunging mesoscopic 'z' folds indicating that the metadolerites, at this point, lie on the upper limb of an east closing synform.

The metadolerites sampled on the western flank of Protectoraksla intrude, however, dark grey to black laminated metacarbonates that lie directly below the thickly bedded Alkhornet-type metacarbonates. Here, the metacarbonates display well exposed decametric, north plunging 'z' folds indicating their presence on the upper limb of an east closing synform.

A small metagabbro lens cropping-out on the coastal cliff 100 m west of the stream issuing from Daudmannsdalen also lies within thin bedded dark grey metacarbonates that are often heavily veined. The dark metacarbonates along the coastal cliffs are occasionally interleaved with strongly crenulated chlorite-carbonate rich phyllites and quartzites. The trend of the F2 crenulation fold axes is very variable ranging from NNE–SSW with northerly plunges to more E–W trends with easterly plunges.

All of the sampled meta-igneous rocks occur as elongate boudins within the syn-metamorphic S1 tectonic foliation that is axial planar to the above large scale F1 folds. Internally the boudins are dissected into smaller lenses with sheared margins oriented at high angles to the main boudin body. These shear surfaces are often decorated with multiple carbonate slickolites. The lenses within the boudins are often massive with more foliated margins. In the Daudmannsdalen area the meta-igneous boudin contacts with the host Alkhorn-like metacarbonates are seen to be highly sheared to mylonitic (Figure 2B–D,G,H). Carbonate veins, often associated with some brecciation, traverse the contact zone into the meta-igneous boudins.

### 3. Fieldwork and Methods

#### 3.1. Fieldwork

The investigated area provided a wide spectrum of metadolerite complexes [24,30,38]. Materials for the investigations here were collected from six sites within the South-Western area of Oscar II Land (Figure 1b). They represent meta-igneous rocks from three separate locations with samples taken from four sites in the Daudmannsdalen area (SW slope of Protektorfjellet), one site from Isfjorden coast (600 m to the east from Ingertrødden) and one site from the western slope of Protektoraksla. A total of 36 oriented "block-samples" (six samples from each site), about 15 cm in diameter, were collected. Metabasic samples were usually taken from the central parts of investigated intrusive sheets that were characterized by a massive texture. Structural observations were conducted in each of the palaeomagnetic sites.

#### 3.2. Petrographic and Mineralogical Methods

Petrographic and mineralogical observations were carried out in transmitted and reflected light. Samples for optical microscopy were prepared from "whole rock" material as well as separates containing ferromagnetic intergrowths. The chemical compositions of the ferromagnetic minerals and backscattered electron (BSE) images were determined using a CAMECA SX 100 electron microprobe (15 kV and 20 nA) at the Electron Microprobe Laboratory (Faculty of Geology, University of Warsaw). Natural and synthetic standards supplied by SPI and CAMECA were used during the analyses.

#### 3.3. Ferromagnetic Minerals Separation

Following the initial petrographic and rock-magnetic analyses two of the metadolerite samples (Dau14, Pro63- sites DAUST2 and PROST6 respectively) were chosen for ferromagnetic minerals separation. The selected samples had the most representative mineral composition and magnetic properties for the whole set of samples. Both samples were crushed (using a Testchem LKS-60) and sieved in the Laboratory of Preparation and Separation of Minerals at the Faculty of Geology, University of Warsaw. The grains were then separated into Ø0.125, Ø0.25 size fractions. The separation of

small particles of metadolerite with minute intergrowths of ferromagnetic phases was carried out using a Frantz isodynamic separator. The Frantz isodynamic separator was set to standard operating conditions [39,40], with the side slope fixed at 15° and the forward slope of the chute was set to 20°. A current of 0.1 A was used to control the intensity of the magnetic field during separation. According to Rosenblum & Brownfield [40] the optimum current values for separation of the ferromagnetic magnetite and pyrrhotite grains is close to 0.01 A. The separated magnetic residuum was dominated by two categories of grains: pyrrhotite (labelled as Dau14-pyrrhotite) and pyrite grains with ferromagnetic intergrowths (labelled as Dau63-pyrite).

#### 3.4. Rock-Magnetic, Anisotropy of Magnetic Susceptibility (AMS) and Palaeomagnetic Methods

From each of the “block-samples” 3 (4 in site DAU1) equally, representative, cores, 2.4 cm in diameter and 2.2 cm in length, were drilled and used for the palaeomagnetic and AMS procedures. Additional cores and powdered samples from each of the sites were prepared for the identification of the ferromagnetic carriers. The rock-magnetic and palaeomagnetic experiments were conducted at the Laboratory of Palaeomagnetism, Institute of Geophysics, Polish Academy of Sciences.

##### 3.4.1. Rock-Magnetic Procedures

- Vibrating Sample Magnetometer (VSM)

The hysteresis parameters including  $M_{rs}$ —saturation magnetization,  $M_r$ —saturation remanence,  $H_c$ —coercivity,  $H_{cr}$ —remanent coercivity, were determined using precise PMC MicroMag 2900 Series AGM Vibrating Sample Magnetometer (VSM) in maximum field 1 T. Hysteresis loops have been measured for the small particles of “whole rock” samples (up to 0.02 g) as well as the separated magnetic grains. All results were normalized against the mass of the samples.

- Temperature dependence of magnetic susceptibility ( $\kappa(T)$ )

The maximum unblocking temperatures ( $T_{ub\ max}$ ) were estimated from the temperature dependence of magnetic susceptibility  $\kappa$  (T measurements). The experiments were conducted on the MFKA1-FA Kappabridge using the high-temperature CS-3 furnace. Analyses were performed on “whole-rock” powder samples representing each of the palaeomagnetic sites. The  $\kappa(T)$  was monitored during continuous heating in air up to 700 °C and during cooling to room temperature.

- Three component IRM (isothermal remanent magnetization) acquisition curve experiment [41]

These procedures produced more detailed information about the ferromagnetic composition. It was possible to observe the contribution of low, medium and high coercivity minerals in the magnetic signal and identify them on the basis of their maximum unblocking temperatures ( $T_{ub\ max}$ ). Initially 12 selected cylindrical samples (2 from each of the sites) were magnetized in steps along the z-axis reaching 3 T. To magnetize the samples a MMPM-10 pulse magnetizer was used. After each level of magnetization, the IRM was measured using the Superconducting Quantum Interface Device (SQUID DC, model 755, 2G Enterprise Inc., Sand City, CA, USA) and then plotted on the diagram. In the next step the samples were magnetized along the other perpendicular axis: along the y-axis in 0.4 T and along the x-axis in 0.12 T, respectively. After magnetization, the samples were gradually thermally demagnetized in the MMTD1 magnetic furnace and measured on the SQUID at every temperature step to determine the decrease of magnetic signal.

##### 3.4.2. Palaeomagnetic Procedures

The experiments began with measurements of the natural remanent magnetization (NRM). The samples then were thermally demagnetized in steps up to 680 °C in the MMTD1 free-field magnetic furnace. After each heating step the residual magnetic field was measured using the SQUID. After each

demagnetization step the magnetic susceptibility of the samples was measured using the low-field KLY 2 susceptibility bridge to monitor any possible formation of new ferromagnetic phases in the samples as a result of the heating. Additionally, several representative samples were demagnetized using the Alternating Field (AF) methods where samples were gradually magnetized up to 160 mT. The low-coercivity components were demagnetized up to 20 mT and labelled AFL. Above 20 mT the high-coercivity components were demagnetized and labelled AFH. The thermal demagnetization in this case was the most effective method of extracting Characteristic Remanent Magnetization (ChRM) components.

### 3.4.3. Statistical Procedures and Software

To calculate the AMS ellipsoids ANISOFT 42 software [42] was used. The demagnetization data were plotted and the ChRM components were calculated using REMASOFT 3.0 software [43] which is based on a principal component analysis (PCA) after Kirschvink [44] and Fisher [45] statistics. To determine the palaeomagnetic components the orthogonal Zijderveld diagrams were used. Palaeomagnetic directions were extracted using “free line fit” and/or “anchored line fit” methods [46] (pp. 121–122) with a maximum angular deviation (MAD) in 90% not exceeding 10°. Only those mean site directions which passed the criteria  $\kappa > 10$ ,  $\alpha_{95} < 17^\circ$  (see discussion regarding number of samples and statistical uncertainties in Van der Voo, 1993 [47]) qualified for further consideration. The site means that qualified were calculated from a minimum of 4 independently oriented block samples (min.  $N = 4$ ). The Virtual Geomagnetic Poles (VGPs) were calculated and compared with the APWP (apparent polar wander path) curves for Baltica, Laurussia and Laurentia using GMAP 2012 software [48]. Additional rotation of palaeomagnetic components reflecting tectonic corrections were conducted using SPHERISTAT 3.2.1. software.

## 4. Results

### 4.1. Petrography of Investigated Metadolerites

The metadolerite protholiths from SW Oscar II Land varied from medium-grained dolerites with well-preserved intersertal textures (Figure 3A,B) to fine-grained samples rich in clinopyroxene phenocrysts (Figure 3C,D). The primary rock-forming assemblages include clinopyroxene, plagioclase, magnetite, ilmenite, pyrrhotite and apatite. Olivine was not found either as phenocrysts or as pseudomorphs. The metamorphic assemblages are represented by albite, chlorite, actinolite, titanite and rare epidote, which unequivocally define the greenschist facies grade of metamorphism. From a petrological point of view the examined metadolerites can be grouped with the Neoproterozoic (?) metabasites described by Michalski et al. [14].

In thin section, all of the metadolerites rocks show a marked alteration of the protolith assemblages (see Figure 3A–F). The feldspars are commonly altered especially to albite where the rocks are foliated (e.g., Figure 3A,B). The pyroxenes show signs of brittle deformation being fragmented along cleavage planes. The pyroxene fragments are strung out into tails from the phenocrysts into the tectonic foliation (Figure 3C–F). Alteration to chlorite along these fracture planes and margins is common while in other cases the pyroxenes are completely retrograded to chlorite and actinolite which is aligned into and defines the metamorphic foliation. Many opaque phases (ilmenite/titanite/pyrite) are evident and some of these also appear fragmented and aligned into the metamorphic foliation (site PROST6, Figure 3E,F).

The meta-gabbro on the coast, south of Daudmannsdalen (site DAUST5), is texturally very variable. In some patches, the original aphyric to intersertal textures are preserved (Figure 3A,B). The feldspars in some samples show random orientations while in others a weak magmatic (?) flow-like texture is preserved. In the latter case the ilmenite/titanite grains are not aligned or fragmented. The pyroxenes may show some alteration but largely preserve a zoned or twinned character. In other patches this meta-gabbro shows complete alteration to greenschist facies parageneses.

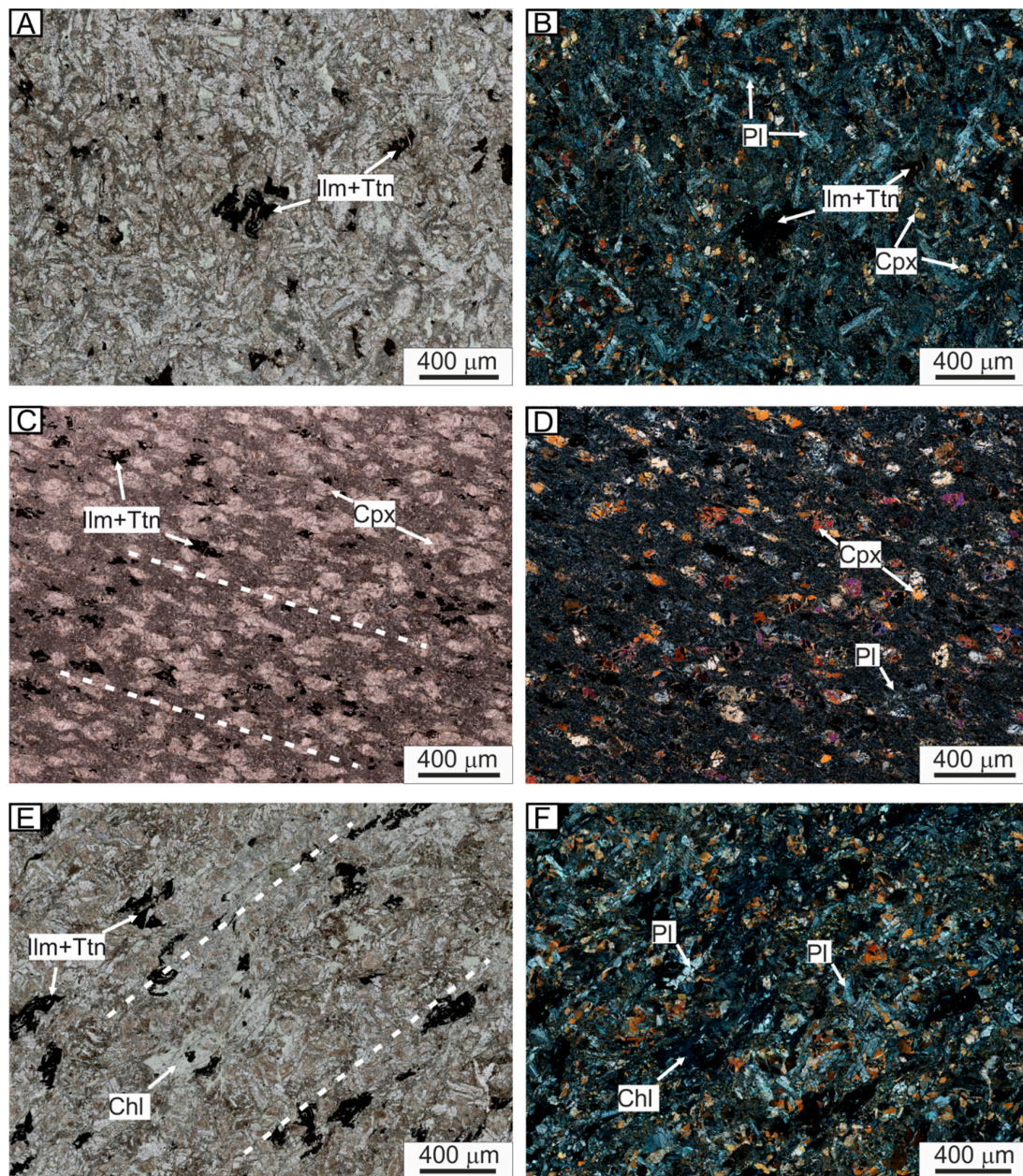


**Figure 3.** (A,B) Single and crossed-nicol photomicrographs of sample Dau5607 (site DAUST5), cropping-out on the coast 100 m SW of the outfall of the stream issuing from Daudmannsdalen. The randomly oriented feldspars are albitic-oligoclase with sericitized margins (A). The pyroxenes appear fragmented and many cases are partially to completely replaced by chlorite (B). The primary magmatic ilmenite/magnetite grains show no preferred orientation. (C,D) Single and crossed-nicol photomicrographs of metadolerite sample Dau1411 (site DAUST2). In this sample, there is a strong preferred orientation of the pyroxenes and the ilmenite/magnetite grains (C). Both show brittle deformation and a sinistral sense of shear. The feldspars are completely sericitized (D). (E,F) Single and crossed-nicol photomicrographs of the metadolerite sample Pro-63 (site DAUST6). In this sample, the ilmenite/magnetite grains are aligned in S1 foliation (E) and they are fragmented. The sample is traversed by NE-SW 2–3 mm wide chlorite bands derived from the alteration of the pyroxenes sheared fragments of which, along with those of feldspars, are entrained in the foliated matrix (F). Foliation planes marked by dashed line. Abbreviations: Chl—chlorite, Cpx—clinopyroxene, Ilm—ilmenite, Pl—plagioclase, Ttn—titanite.

## 4.2. Identification of Ferromagnetic Minerals

### 4.2.1. Mineralogical Methods

Metadolerites representing all of the palaeomagnetic sites were examined in thin section (12 samples) to determine the compositions of the ferromagnetic phases and their associations. While the ferromagnetic associations of the metadolerites were found to be mineralogically comparable they do differ texturally (Figure 3). The ferromagnetic phases that were identified occurred only as accessory components of the metadolerites. Usually, they appear to have crystallized contemporaneously with other non-magnetic ore minerals (Figure 4A–E). However, ferromagnetic phases often occurred as tiny inclusions within major rock-forming pyroxenes and metamorphic epidotes (Figure 4F).

Regardless of the textural diversity of the samples all primary magmatic ferromagnetic components (e.g., Ti-rich magnetite) were recrystallized or replaced by metamorphic sulphides and/or titanite during the low-grade Caledonian (*sensu lato*) metamorphism (Figure 4A–F). The degree of primary ilmenite transformation depends on the dynamic recrystallization processes (Figure 3). A small amount of metamorphic magnetite, up to 3  $\mu\text{m}$  in diameter (Figure 4F), was found as minute intergrowths within metamorphic aluminosilicate grains. Most magnetite intergrowths are of sub-microscopic size and were unsuitable for EPMA analysis. The presence of magnetite within the examined samples has also been confirmed by rock-magnetic experiments. The presence of the above ferromagnetic Fe-oxides has proven to be common in the metamorphic basement of western Spitsbergen [13–15,49,50]. In many thin sections, small amounts of anatase were also found (Figure 4C). The Fe-Ti-associations, represented by ilmenite, anatase and titanite record low grade metamorphic processes under high  $\text{H}_2\text{O}$  activity and  $f\text{O}_2$  fugacity [51–56].

The main ferromagnetic carrier identified in the metadolerites is pyrrhotite (Figure 5A,C–E). This mineral occurs in varying amounts in particular palaeomagnetic sites and usually occurs in parageneses with pyrite (Figure 5A–F). In samples from Daudmannsdalen (sites DAUST1-4), where more metamorphic textures are well expressed, pyrrhotite was rarely observed and then only as tiny intergrowths in larger pyrite grains (Figure 5A). A common component of sulphide parageneses is chalcopyrite (Figure 5A–C,E). The sulphides in most sites are often surrounded by Fe-hydroxides (Figures 4A and 5F). Samples from the Isfjorden coast (site DAUST5), with a preserved magmatic texture, are very rich in pyrrhotite, which occurs as intergrowths in clinopyroxenes and/or titanite (Figure 5D,E) as well as large separated aggregates that have grown together with chalcopyrite (Figure 5C). The textural varieties of the pyrrhotite, especially as intergrowths with the aluminosilicates indicates that it is of metamorphic origin. The latest mineral phases within the sulphide associations are represented by goethite (Figure 5A,F). The presence of Fe-hydroxides is suggestive of low-temperature alteration during metamorphism than weathering as in some places goethite is rimmed by, or included within, the titanite (Figure 4A).

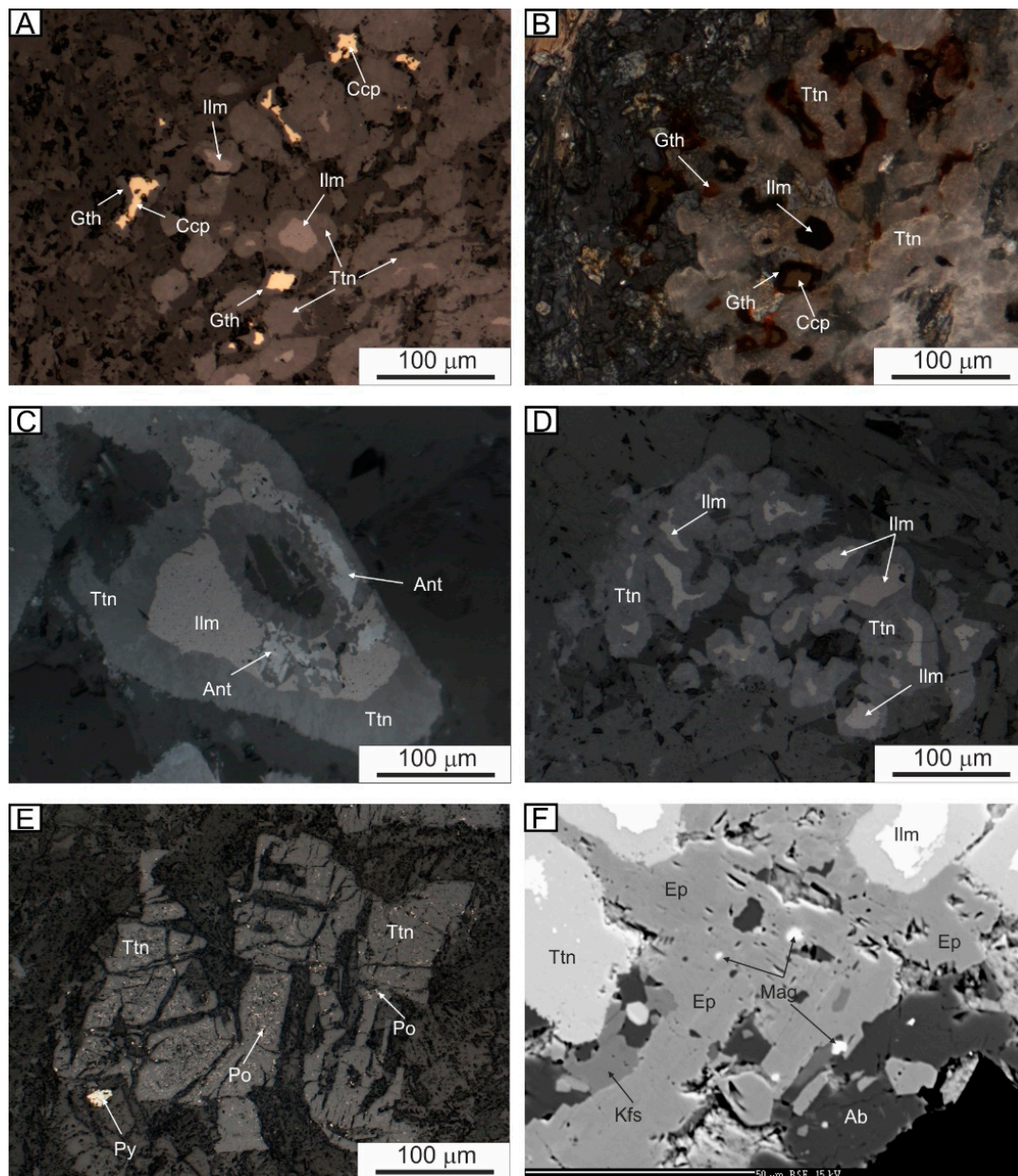


**Figure 4.** Fe-Ti oxides within the metadolerites. (A,B) Ilmenite and chalcopyrite intergrowths partly replaced by metamorphic titanite and goethite, respectively. (A) Sample Dau0109 (site DAUST1), parallel nicols; (B) from the same sample, crossed nicols; (C) Relic of ilmenite surrounded by younger titanite and anatase. Sample Dau-1219 (site DAUST2), parallel nicols; (D) Metamorphic titanite growing around ilmenite. Sample Dau5304 (site DAUST5), parallel nicols; (E) Titanite pseudomorph after Ti-magnetite (magmatic in origin). Within titanite numerous irregular inclusions of metamorphic pyrrhotite. Sample Dau5607 (site DAUST5), parallel nicols; (F) BSE image showing small euhedral magnetite crystals within epidote. Ilmenite surrounded by titanite, small intergrowths of albite and K-feldspars. Sample Dau14 (site DAUST2). Abbreviations: Ab—albite, Ant—anatase, Ccp—chalcopyrite, Ep—epidote, Gth—goethite, Ilm—ilmenite, Kfs—K-feldspar, Mag—magnetite, Py—pyrite, Po—pyrrhotite, Ttn—titanite.

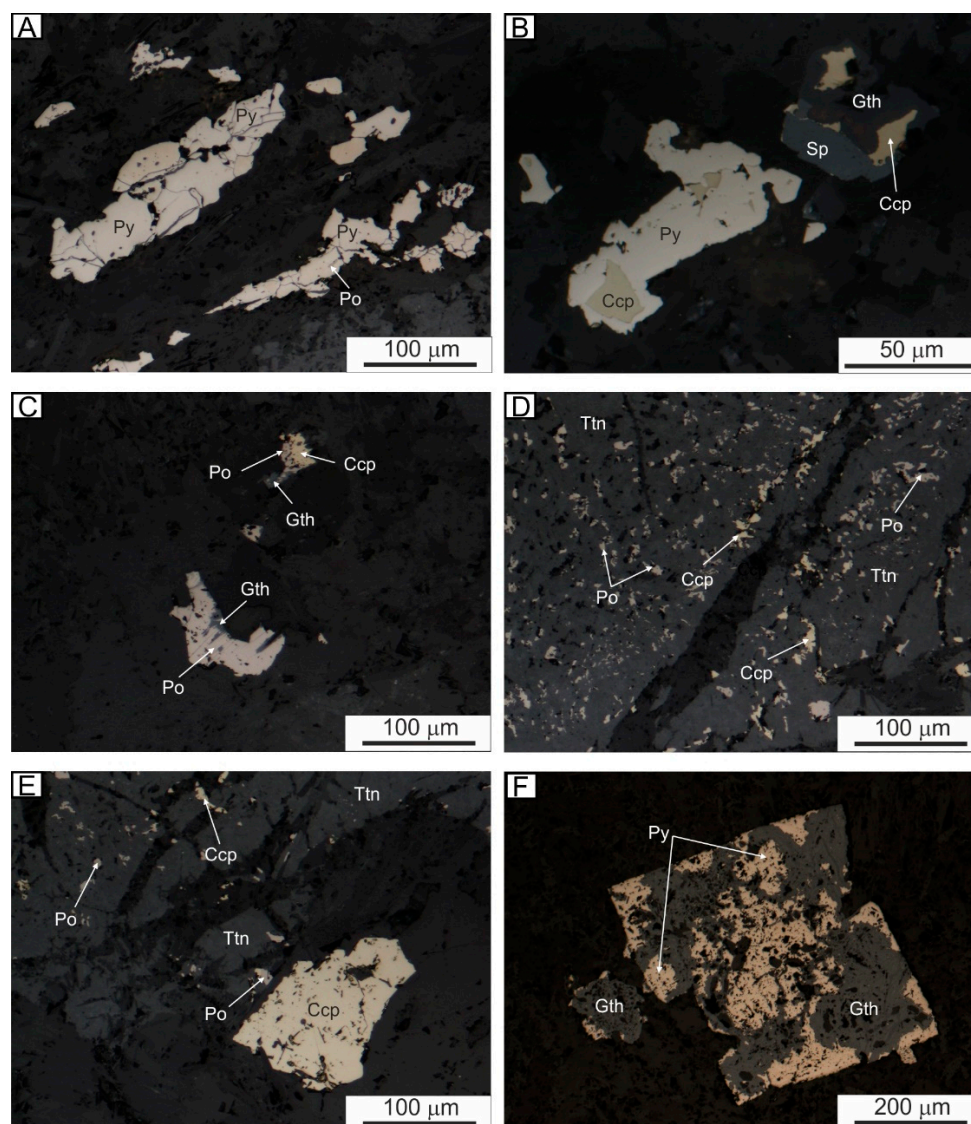


**Figure 5.** Sulphide associations within the metadolerites. (A,B) Pyrite aggregates along the D1–S1 foliation plane. Within the pyrites small blebs of pyrrhotite are common. Sample Dau1411 (site DAUST2), parallel nicols; (B) pyrite, chalcopyrite and sphalerite association. Chalcopyrite is partly replaced by goethite. Sample Dau1411 (site DAUST2), parallel nicols; (C) large pyrrhotite and pyrrhotite-chalcopyrite aggregates. All sulphides are partly replaced by goethite. Sample Dau5304 (site DAUST5), parallel nicols; (D) Titanite pseudomorph after Ti-rich magnetite. Within titanite numerous small blebs of pyrrhotite and chalcopyrite. Sample Dau5607 (site DAUST5), parallel nicols; (E) metamorphic chalcopyrite and titanite with fine inclusions of pyrrhotite and chalcopyrite. Sample Dau5607 (site DAUST5), parallel nicols; (F) euhedral pyrite partly replaced by later goethite. Sample Dau0109 (site DAUST1), parallel nicols. Abbreviations: Ccp—chalcopyrite, Gth—goethite, Py—pyrite, Po—pyrrhotite, Sp—sphalerite, Ttn—titanite.

#### 4.2.2. Rock-Magnetic Experiments

The first step in this part of the investigation was to determine the parameters of the hysteresis loops. In all analysed samples (“whole-rock” and separates) the shape of the loops, after correction for paramagnetics, was characteristic for ferromagnetic phases (Figure 6). The magnetic parameters shown in the Table 1 indicated the dominance of low-medium coercivity fractions ( $H_{cr}$  from 3 mT up to 35 mT). The extraction of ferromagnetic phases from the meta-igneous samples effectively raised the

magnetic signal and allowed the hysteresis loops to be obtained with a lesser influence of paramagnetic minerals (Figure 6G,H).

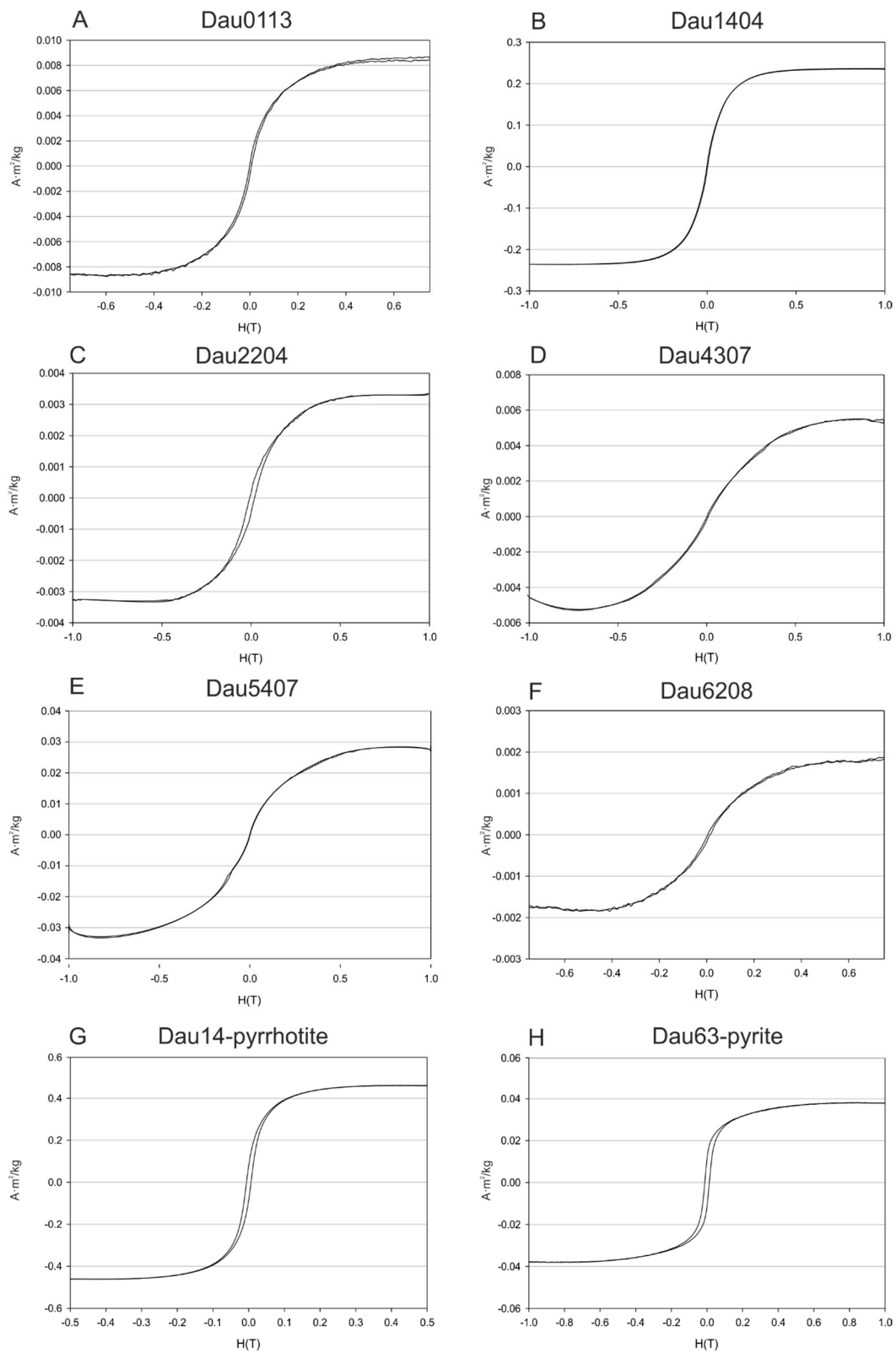


**Figure 6.** Examples of hysteresis loops of “whole-rock” samples (A–F) and separated magnetic fraction (G,H) of metadolerites from SW Oscar II Land.

**Table 1.** Hysteresis parameters of investigated separates and “whole-rock” samples of metadolerites from SW Oscar II Land.  $M_s$ —saturation magnetization;  $M_r$ —saturation remanence;  $H_c$ —coercivity;  $H_{cr}$ —remanence coercivity.

No.	Samples	Description	$M_s$ (A m <sup>2</sup> /kg)	$M_r$ (A m <sup>2</sup> /kg)	$H_c$ (mT)	$H_{cr}$ (mT)	$M_r/M_s$	$H_{cr}/H_c$
1	Dau0113	“whole-rock”–metadolerites	$4.09 \times 10^{-3}$	$4.55 \times 10^{-4}$	4.02	8.34	0.11	2.07
2	Dau1404		$1.66 \times 10^{-2}$	$8.09 \times 10^{-4}$	3.25	8.03	0.05	2.47
3	Dau2204		$3.39 \times 10^{-3}$	$3.47 \times 10^{-4}$	13.39	29.48	0.10	2.20
4	Dau4307		$5.21 \times 10^{-3}$	$4.00 \times 10^{-4}$	3.97	9.25	0.08	2.33
5	Dau5407		$2.29 \times 10^{-2}$	$6.52 \times 10^{-3}$	2.22	7.66	0.29	3.45
6	Pro6208		$3.33 \times 10^{-3}$	$4.45 \times 10^{-4}$	7.81	35.50	0.13	4.55
7	Dau14-63-Po	metadolerite-pyrrhotite 1	$4.61 \times 10^{-1}$	$8.26 \times 10^{-2}$	6.42	11.41	0.18	1.78
8		metadolerite-pyrrhotite 2	$1.46 \times 10^{-1}$	$5.23 \times 10^{-2}$	8.41	9.79	0.36	1.16
9		metadolerite-pyrrhotite 3	$2.99 \times 10^{-2}$	$9.94 \times 10^{-3}$	6.66	9.57	0.33	1.44
10	Dau14-63-Py	metadolerite-pyrite 1	$3.78 \times 10^{-2}$	$1.14 \times 10^{-2}$	12.93	16.01	0.30	1.24
11		metadolerite-pyrite 2	$3.86 \times 10^{-1}$	$1.43 \times 10^{-1}$	11.10	12.90	0.37	1.16

All of the analysed samples were characterized by low initial values of magnetic susceptibility (below  $120 \times 10^{-6}$ ). The results of  $\kappa(T)$  experiments on the metadolerites revealed a similar behaviour for all of the samples during heating and showed the existence of pyrrhotite and magnetite/maghemite with  $T_{ub\ max}$  around 320 °C (Figure 7, sample Dau5401) and 580–600 °C respectively (Figure 7, all samples). An increase in the susceptibility is recorded by the heating curves in the 400–580 °C temperature range which, in the case of the sample Dau4609, is most visible and which may be a Hopkinson effect [57]. The irreversible character of the heating-cooling curves (new ferromagnetic phases observed on cooling curve around 300 °C, Figure 7, for example, sample Dau2601, Dau4609) and higher values of magnetic susceptibility observed on the cooling curves is probably related to the formation of new ferromagnetic phases during sulphides oxidation and/or chemical and mineralogical alteration of paramagnetic minerals [58,59]. The above observations confirmed the results of the susceptibility ( $\kappa$ ) experiments that were monitored during the palaeomagnetic procedure demonstrating that, around 450 °C, the samples became magnetically unstable.

The existence of soft-medium coercivity fractions in the metadolerites rocks has been confirmed by the IRM acquisition curves diagram (Figure 8). They were mostly saturated in low-medium fields about 0.5 T.

Lowrie diagrams for all samples show a distinct domination of low and medium coercivity minerals assigned to the curves that saturated up to 120 mT and in the range 120–400 mT respectively. Moreover, the diagrams revealed a complex character of demagnetization with several distinct temperatures in ranges 200–275 °C, 300–375 °C, 400–450 °C and 500–560 °C (Figure 9). The first range 200–275 °C could be correlated with sub-microscopic grains of magnetite or maghemite characterized by low values of  $T_{ub\ max}$  [60,61]. The second range 300–375 °C is clearly visible on diagrams Dau2612, Dau4308 (Figure 9) and is interpreted to be related to the demagnetization of pyrrhotite [62]. The last two ranges 400–450 °C and 500–560 °C are probably evidence of the presence of magnetite and/or maghemite. The reason for the occurrence of magnetites with lower demagnetization temperatures than  $T_{ub\ max} = 575$  °C could be the varied grain sizes of this mineral [63].

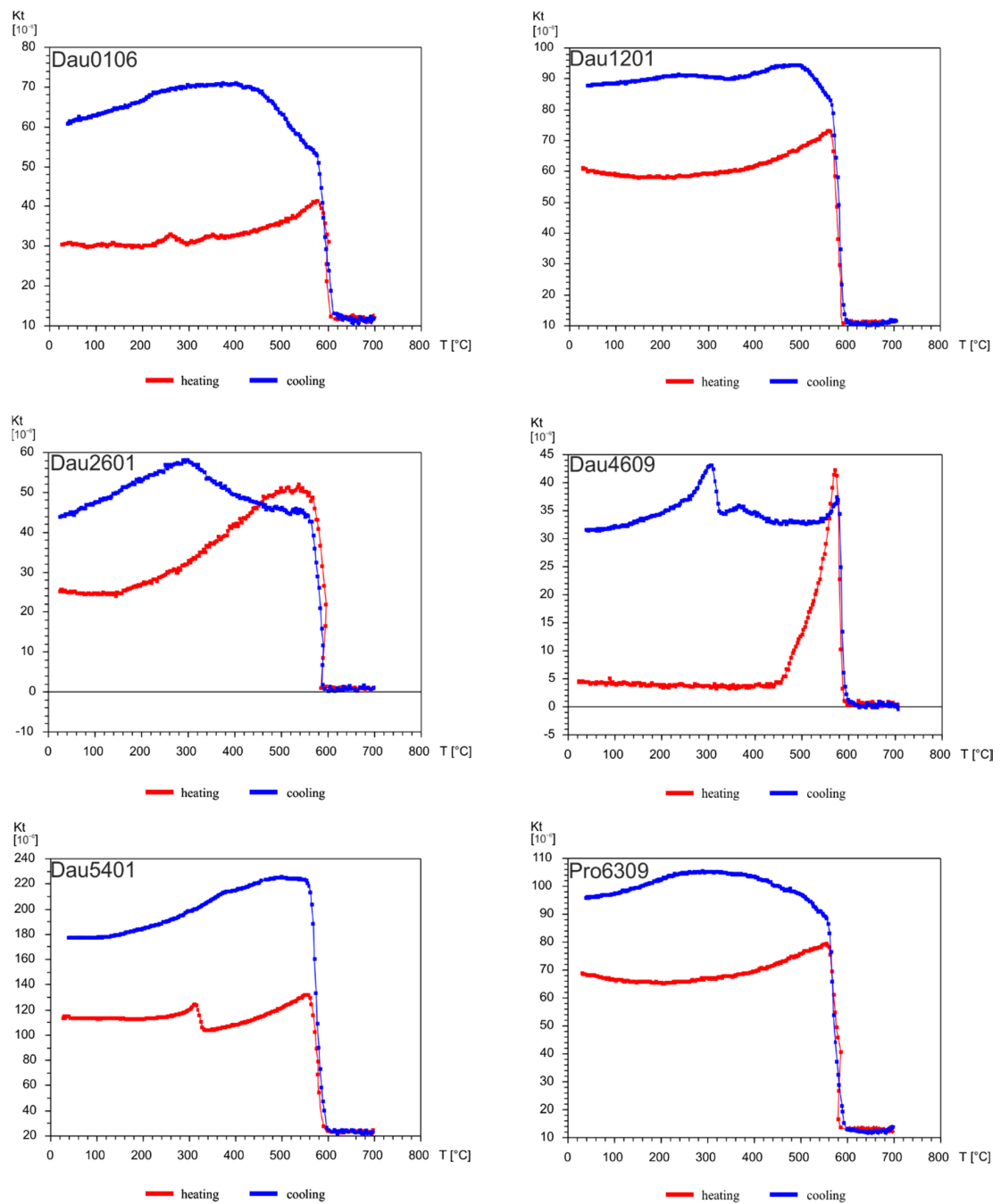


**Figure 7.** Temperature dependence of magnetic susceptibility for metadolerites “whole-rock” samples from south-western Oscar II Land, western Spitsbergen.

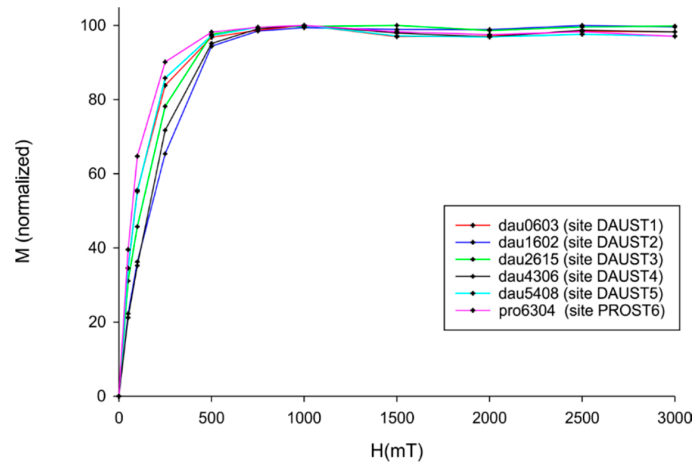


**Figure 8.** Results of isothermal remanent magnetization (IRM) acquisition curves experiments of metadolerites from SW Oscar II Land.

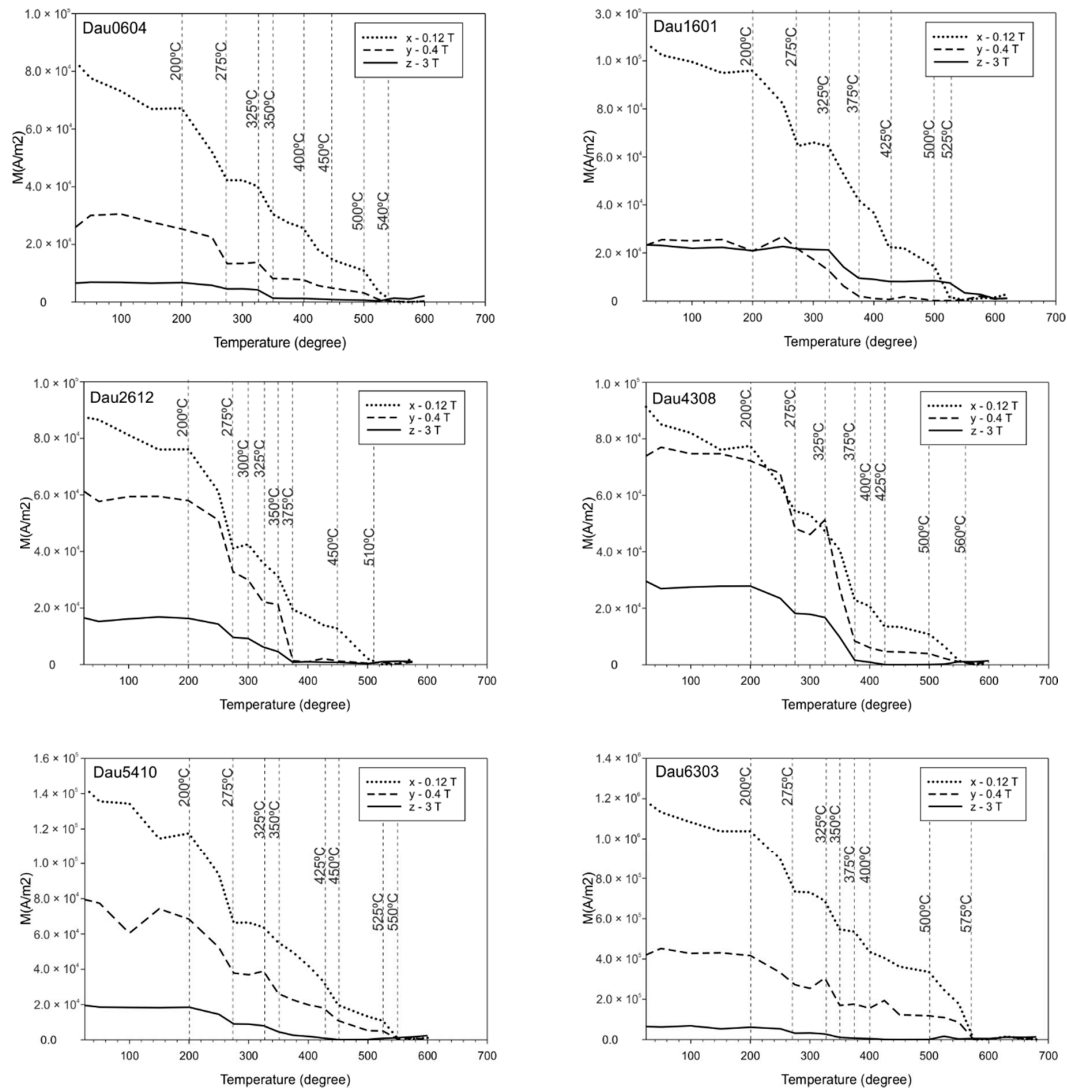


**Figure 9.** Results of three component IRM acquisition curve experiments [28] of the metadolerites of SW Oscar II Land.

### 4.3. Palaeomagnetic Results

The analysed metadolerites revealed low initial values of the NRM intensities ranging between, in most cases, 0.1–1.5 mA/m. Only a few samples from sites DAUST5 and PROST6 reached the 50 mA/m value.

In the course of the thermal demagnetization procedure (Figure 10) the low-field magnetic susceptibility was monitored. Initially, the mean values of susceptibility of the meta-igneous samples ranged from  $8.5 \times 10^{-4}$  to  $1.0 \times 10^{-3}$  SI. In all of the investigated samples the susceptibility was stable up to 500 °C. Above 500 °C an increase of the magnetic susceptibility was observed accompanied by an increase in the NRM intensity and a disturbance of the NRM pattern which prevented any further identification of the palaeomagnetic components. The observed phenomenon can be explained by the formation of new ferromagnetic minerals in the samples for example, oxidation of Fe-sulphides to magnetite [63], in the course of the thermal experiments.

Using Principal Component Analysis (PCA) the following NRM components, distinguished by different ranges of unblocking temperatures ( $T_{ub}$ ), were characterized:

- (1) A low temperature component (index L) which demagnetized below 250 °C, was calculated using the “free line fit” method of Butler [46]. This was characterized by a steep inclination that was probably influenced by the present-day magnetic field.
- (2) A medium temperature component (index M) which demagnetized in the 250–350 °C range of temperatures and calculated using the “free line fit” or the “anchored line fit” methods of Butler [46], was potentially related to pyrrhotite and/or magnetite/maghemite grains of relatively low- $T_{ub}$ , that were identified during the petrological and rock-magnetic experiments.
- (3) A high temperature component (index H) which demagnetized above 350 °C and up to 500 °C (before disturbance of the NRM pattern). That component was also calculated using the “free line fit” or the “anchored line fit” methods [46] and is potentially related to magnetite and/or maghemite grains with higher a  $T_{ub}$  spectra than was the case for the M component.

In three of the sites selected components were demagnetized over 250–500 °C range of temperatures. Such multi-components were labelled MH and they were calculated using only the “anchored line fit” method [46].

The majority of the analysed L components were well grouped ( $\kappa > 25$ ,  $\alpha_{95} < 9^\circ$ ) except PRO6L where the mean L component was imprecisely defined (Figure 11A, Table 2). In contrast, only two of components demagnetised in temperatures  $\geq 250$  °C passed accepted statistical criteria— $\kappa > 10$ ,  $\alpha_{95} < 17^\circ$  (DAU2MH+, DAU4MH+, Figure 11B, Table 2). All other middle—high temperature components were much less clustered ( $\kappa < 10$ ,  $\alpha_{95} > 25^\circ$ ) and were rejected from further interpretation. Scattering of the middle-high temperature components in the majority of the sites will be discussed below. None of the components extracted by the AF method qualified for further analysis.

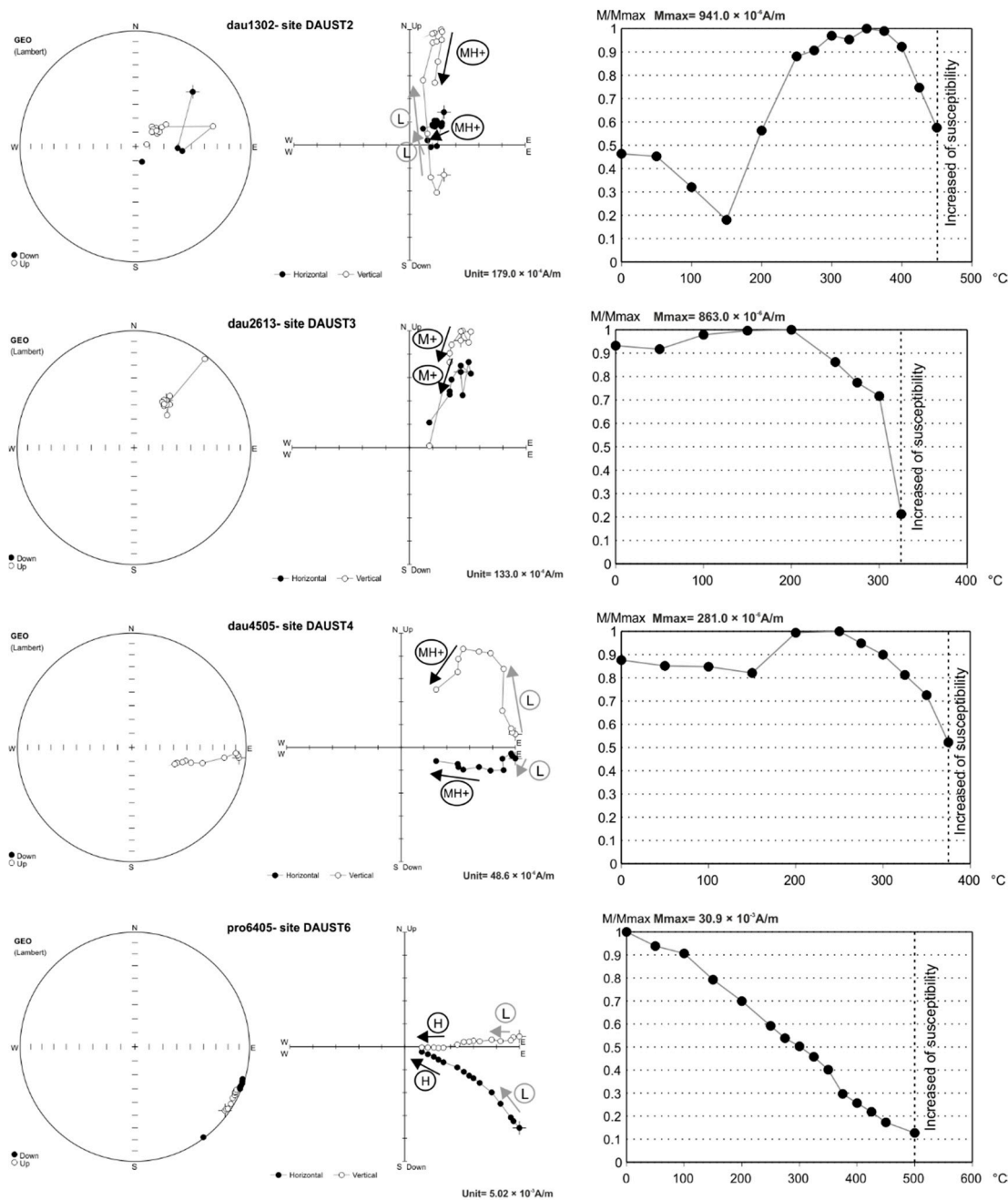


**Figure 10.** Examples of the most characteristic demagnetization diagrams used to calculate palaeomagnetic site mean directions of metadolerites from SW Oscar II Land. Left column—equal area; middle column—Zijderveld diagrams; right column—normalized intensity decay plots; diagrams are presented for in situ orientation; on equal area points located on upper and lower hemisphere were marked as open and filled symbols respectively; on Zijderveld diagrams open and filled symbols means projections onto vertical and horizontal planes correspondingly, low components marked by grey arrows, medium-high components marked by black arrows, components calculated using the “anchored line fit” method marked by “+”.

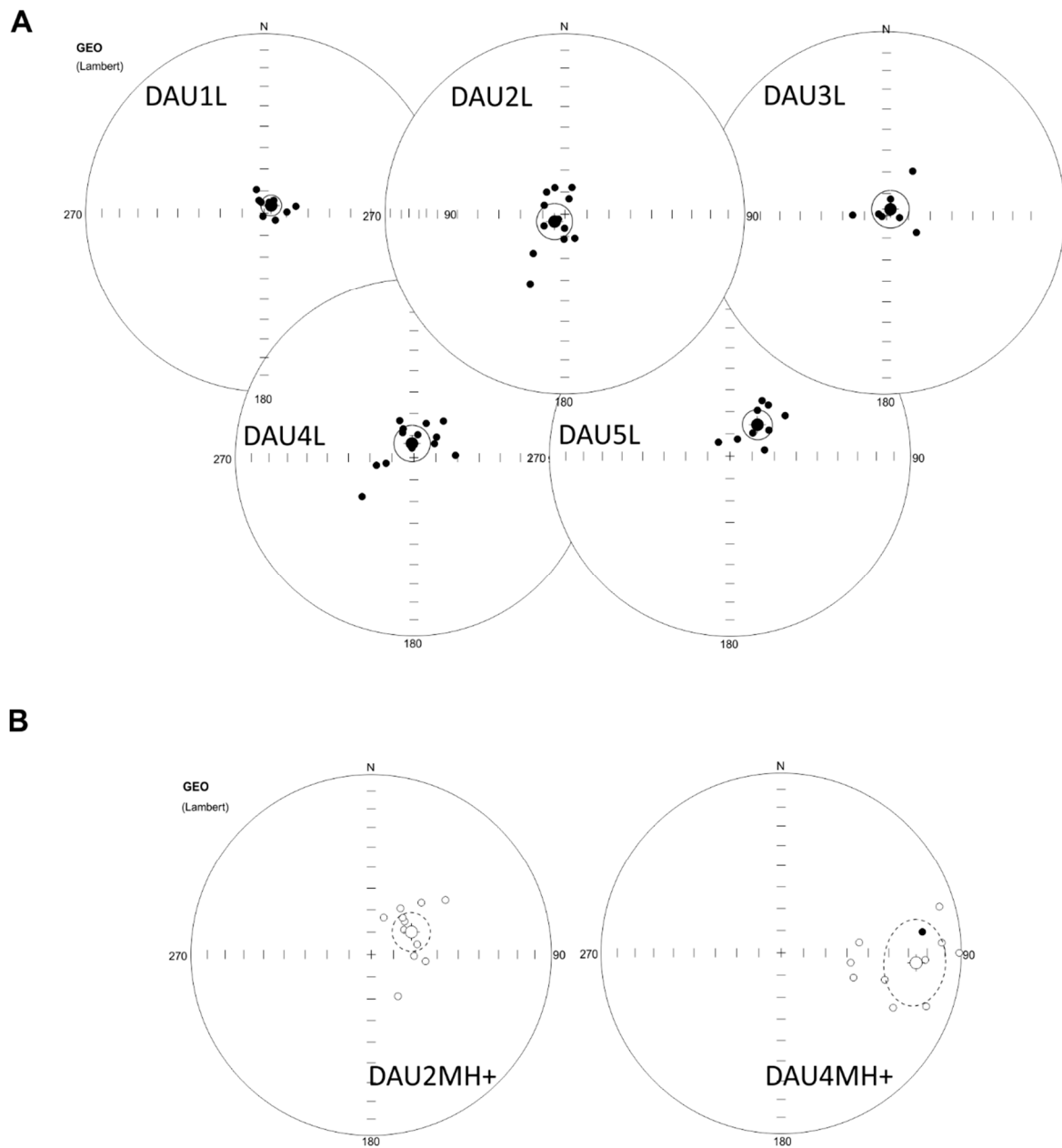


**Figure 11.** (A) Low temperature NRM components, (B) Medium-high temperature NRM components on equal area projections representing metadolerites sites from SW Oscar II Land. All of the components presented passed statistical criteria— $\kappa > 10$ ,  $\alpha_{95} < 17^\circ$  and were accepted for further interpretation. Open and full symbols correspond to upper and lower hemisphere respectively. Site mean directions with their radiuses of 95% confidence circles are presented. Specification of palaeomagnetic parameters is summarized in Table 2.

**Table 2.** Statistical parameters of the palaeomagnetic components identified in metadolerite samples of SW Oscar II Land. Components characterized by  $\alpha_{95} > 90^\circ$  are not shown in the table. Explanations: L component  $< 250^\circ\text{C}$ ; M component  $250\text{--}350^\circ\text{C}$ ; H component  $> 350^\circ\text{C}$ ; AFL component  $< 20\text{ mT}$ ; AFH component  $> 20\text{ mT}$ ; + components calculated using “anchored” line fit method [46]; D—declination; I—inclination; S—total number of independently oriented hand samples subjected to demagnetization; s—total number of demagnetized specimens; N/n—number of independently oriented hand samples/specimens used for Fisher statistics;  $\alpha_{95}$ —radius of 95% confidence circle;  $\kappa$ —Fisherian precision parameter; components with  $\alpha_{95} < 17^\circ$  has been qualified for further tectonic consideration.

Site	Site GPS Location	Components	D (°)	I (°)	S/s	N/n	$\alpha_{95}$	$\kappa$
DAU1	N78°12'32.8 E13°40'24.9	DAU1L	42.7	85.3	6/22	4/9	4.7	120.7
DAU2	N78°12'33.1 E13°40'38.9	DAU2AFL	348.4	74.5	5/5	4/4	31.0	9.73
		DAU2L	234.6	84.4	6/18	5/12	8.1	29.64
		DAU2MH+	60.9	−69.2	6/18	5/11	8.6	28.84
DAU3	N78°12'33.3 E13°40'48.3	DAU3L	310	86.5	6/18	5/8	8.5	43.21
		DAU3M+	85.8	−16.8	6/18	4/9	27.0	4.58
DAU4	N78°12'5.7 E13°41'20.9	DAU4L	352.6	83.5	6/18	5/13	8.2	26.25
		DAU4MH+	94.2	−25.8	6/18	5/11	16.5	8.63
DAU5	N78°11'52.4 E13°40'04.1	DAU5L	41.3	71.2	6/18	5/10	6.7	52.65
		DAU5AFL	30.7	81.3	6/7	4/4	84.5	2.17
		DAU5MH+	59.2	−53.2	6/18	6/12	33.2	2.67
PRO6	N78°13'56.8 E13°41'42.6	PRO6L	108.8	29.3	6/18	4/5	40.4	4.53
		PRO6H	114.2	−13.0	6/18	4/5	37.1	5.21

## 5. Discussion

The rock- magnetic studies have revealed that ferromagnetic carriers in the metadolerites from SW OIIL are dominated by metamorphic pyrrhotite and Fe-oxides. The results of the petrological—mineralogical analyses strongly suggest a lack of any relicts of pre-metamorphic ferromagnetic minerals. All of the primary magmatic Fe-, Fe-Ti-oxides have been replaced by metamorphic titanite and anatase (Figure 4C).

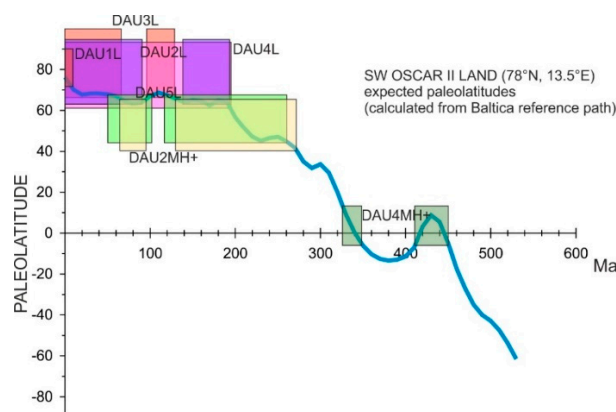


**Figure 12.** Palaeolatitudes of Western Terrane of Svalbard (*sensu* Harland 1997 [26]) during magnetization of palaeomagnetic components identified in metadolerites of SW Oscar II Land; palaeolatitude curve for Oscar II Land sampling area ( $78^\circ\text{ N}$ ,  $13.5^\circ\text{ E}$ ) has been calculated from Baltica APWP, derived from GMAP 2012 palaeopoles libraries [48]; all palaeolatitudes of investigated area are recalculated for northern hemisphere and are presented with confidence limits defined by  $D_p$  (half-axis of palaeopole oval of the confidence limit  $\alpha_{95}$ ).

The  $L T_{ub}$  palaeomagnetic components are defined precisely in the majority of the sampled sites except for PROST6 (Table 2). The palaeolatitudes and Virtual Geomagnetic Poles (VGP) analyses (Figures 12 and 13, Table 3) indicate that the  $L T_{ub}$  components are products of a Mesozoic–Cenozoic remagnetization.

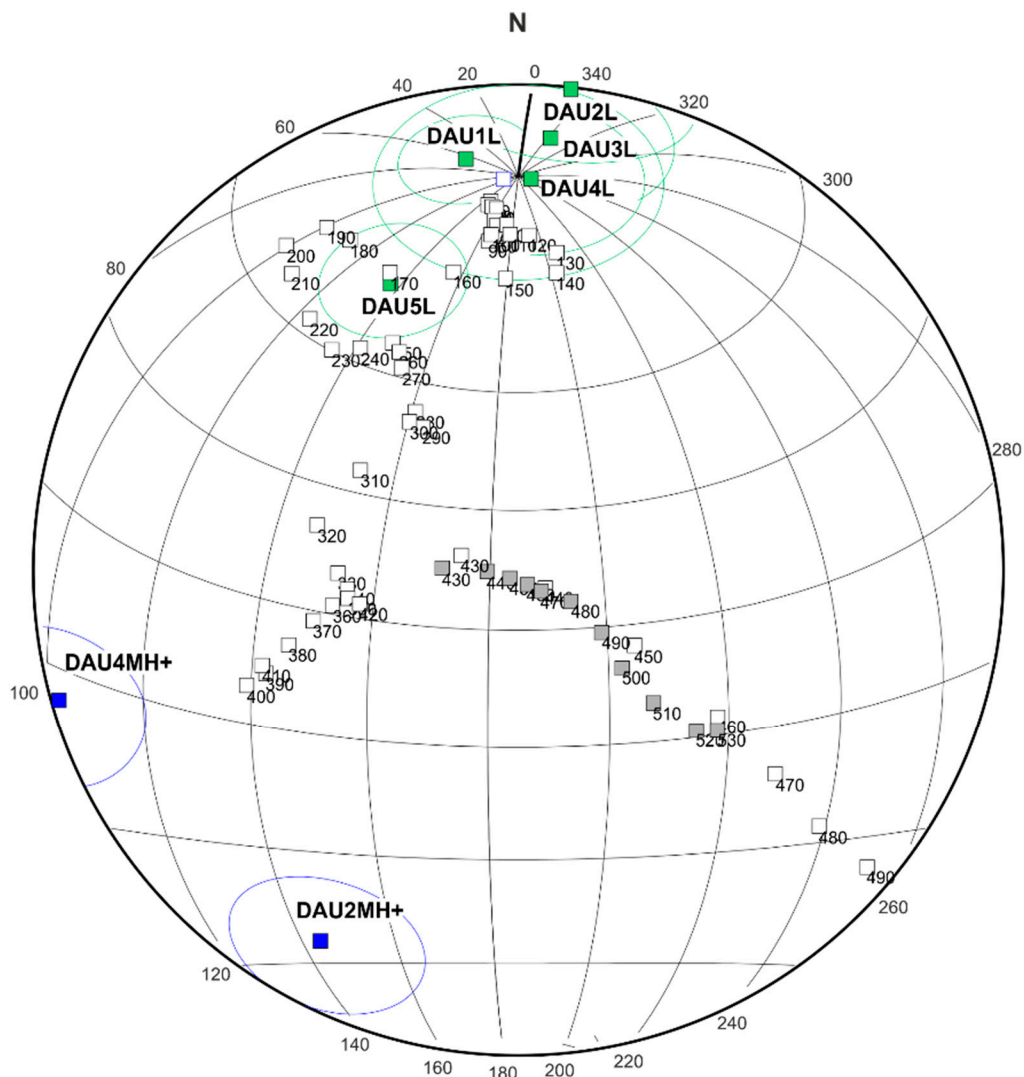


**Figure 13.** Schmid projection of VGPs calculated for all site mean components with  $\kappa > 10$ ,  $\alpha_{95} < 17^\circ$  identified in SW Oscar II Land metabasic rocks with their ovals of the confidence limit  $\alpha_{95}$  against reference path of Laurussia (open squares, palaeopoles 0–430 Ma), Baltica (open squares, palaeopoles 440–530 Ma) and Laurentia (filled squares, palaeopoles 440–530 Ma); reference palaeopoles was taken from Torsvik et al. [48]; ages of particular palaeopoles are given.

**Table 3.** VGPs calculated for components identified in metadolerites from SW Oscar II Land, Western Spitsbergen (average sampling location 78° N, 13.5° W), qualified for further tectonic interpretation ( $\kappa > 10$ ,  $\alpha_{95} < 17^\circ$ ; Table 2). Explanations: P—polarity (N—normal; R—reverse);  $\Phi$ —palaeopole latitude;  $\Lambda$ —palaeopole longitude; Dp/Dm—half-axes of palaeopole oval of the confidence limit  $\alpha_{95}$ ; Plat—palaeolatitude; other abbreviations as in Table 2.

VGP Symbol	N	n	P	D (°)	I (°)	$\alpha_{95}$	$\kappa$	$\Phi$ (°) N	$\Lambda$ (°) E	Dp/Dm (°)	Plat (°)
DAU1L	4	9	N	42.7	85.3	4.7	120.7	81.88	64.68	9.2/9.3	80.7
DAU2L	5	12	N	234.6	84.4	8.1	29.64	69.50	346.89	15.8/16.0	78.9
DAU2MH+	5	11	R	60.9	−69.2	8.6	28.84	−45.86	144.12	12.5/14.7	52.8
DAU3L	5	8	N	310	86.5	8.5	43.21	80.80	337.92	16.8/16.9	83.0
DAU4L	5	13	N	352.6	83.5	8.2	26.25	88.20	259.41	15.8/16.1	77.2
DAU4MH+	5	11	R	94.2	−25.8	16.5	8.63	−14.16	102.27	9.6/17.8	13.6
DAU5L	5	10	N	41.3	71.2	6.7	52.65	63.69	136.55	10.2/11.7	55.8

In contrast, the M/H/MH  $T_{ub}$  components from four of the six investigated sites are scattered ( $\alpha_{95} > 25^\circ$ ,  $\kappa < 6$ ). Only for the DAUST2 and 4 sites could the middle to high temperatures MH+  $T_{ub}$  mean directions be calculated precisely ( $\alpha_{95} < 17^\circ$ ,  $\kappa > 10$ ) qualifying them for further interpretation. It should be noted that, despite the differences in the definition of the middle to high temperatures palaeomagnetic components, all of the sites are characterised by well-defined AMS ellipsoids (Appendix A, Figure A1). This particular observation strongly suggests that the AMS only stabilised after some small-scale tectonic rotations had been superimposed on the host metacarbonates. Whatever mechanism was responsible for the alignment of the AMS axes it must have influenced any previous palaeomagnetic directions and could explain the scattering of the M/H/MH components in sites DAUST1, 3, 5 and PROST6. The failure of the experiments in the selected sites can be related also to the complex nature of the ferromagnetic mineralogy and the overlapping of the  $T_{ub}$  spectra of particular components existing in the same samples.

The question arises as to the age of the MH+ magnetization which has survived in sites DAUST2 and 4. Very preliminary considerations regarding their origin are posted below.

The in-situ VGPs for DAU2MH+, DAU4MH+ are definitely shifted from the combined Laurussia-Baltica-Laurentia reference paths. In-situ  $40\text{ Ar}/39\text{ Ar}$  age determinations of the rocks in the adjacent Forlandsundet and Kongsfjorden areas suggest that three thermal events could have, potentially, influenced the palaeomagnetic record of OIIL. The first of these thermal events in the 426–380 Ma interval would represent the Caledonian (*sensu lato*) metamorphism, while the 377–326 Ma and circa 300 Ma ages could represent rift related elevated heat flow events [14,64]. But it is uncertain as to whether the DAU2MH+, DAU4MH+ magnetizations relate to any of the aforementioned thermal episodes. From the structural and petrological data presented here it is evident that the Caledonian tectono-metamorphism was the most important event that could have affected the studied rocks and could have reset their palaeomagnetic record. However, bringing back DAU2MH+, DAU4MH+ site means to the Caledonian *sensu lato* or 380–300 Ma sectors of the reference path of directions expected for area of SW Oscar II Land if it constituted part of Baltica (Figure 14) requires additional, significant, rotations which are not considered by any of the rotational models tested by Michalski et al. [14]. Indeed, the areas of Daudmannsdalen, Daudmannsøyra, Protectorbreen have been shown here to include structurally high strain zones both between and within the metadolerites and their host rocks. The resultant shearing could definitely generate further rotations in addition to the 40° westward dipping listric faulting proposed for central-western Spitsbergen by Michalski et al. [14].

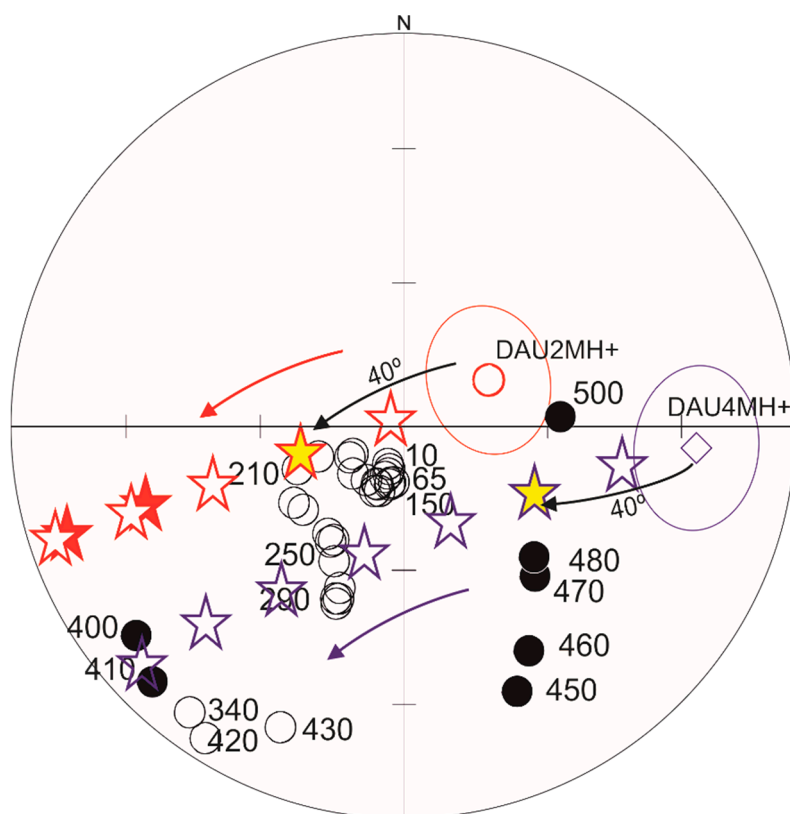


**Figure 14.** Equal area projections of DAU2MH+ and DAU4MH+ palaeomagnetic components with their ovals of the confidence limit  $\alpha_{95}$  against reference path of palaeomagnetic directions expected for area of SW Oscar II Land if it constituted part of Baltica in the Phanerozoic; stars represents gradual rotation of palaeomagnetic components around horizontal axis N  $160^\circ$ , oriented parallel to the West Spitsbergen Fold and Thrust Belt–Knipovich Ridge trend; red and blue arrows pointing to direction of rotation according to listric faulting; stars filled in yellow marked rotation by an angle of  $40^\circ$ .

## 6. Conclusions

- (1) The results of rock-magnetic and petrological analyses, including experiments on ferromagnetic separates, reveal a dominance of metamorphic pyrrhotite and Fe-oxides carriers in the metadolerites of SW OIIL and show complete remineralization and reorganization of their ferromagnetic fabric during Caledonian *sensu lato* metamorphism and younger tectono-thermal events.
- (2) Field data together with an analysis of satellite images (available from the NPI Kart over Svalbard) have highlighted the presence previously unreported deformational features such as large and small-scale folding and the presence of high strain (shear) zones in the Daudmannsdalen, Daudmannsøyra, Protectorbreen sites. All of these features have the potential to influence the orientation of the palaeomagnetic signal carriers.
- (3) The results of the palaeomagnetic investigations are as follows:
  - a. In five of the six sites the low temperature components ( $T_{ub} < 250^\circ\text{C}$ ) are characterised by high inclinations ( $\sim 70^\circ\text{--}80^\circ$ ) and are related to Mesozoic–Cenozoic remagnetization, probably influenced by the recent magnetic field.
  - b. In four of the six sites the middle-high temperature components ( $T_{ub} > 250^\circ\text{C}$ ) were scattered and thus rejected for further consideration. Only from two sites did the middle-high temperature directions qualify. Palaeopoles calculated for these two sites are shifted from combined reference Laurussia–Baltica–Laurentia APWP. At this stage of the

study it is not possible to precisely define origin of observed inconsistency. Potentially the shift of the qualified DAU2MH+, DAU4MH+ VGP's from the reference path can be related to L. Mesozoic–Cenozoic listric faulting of the Caledonian basement, postulated in the area of OIIL by Michalski et al. [14]. Additional rotations could be generated by localised shearing and the cumulative effects of localised west-dipping families of small scale faults which were observed in the sampling area.

- (4) Finally, it is evident, that to better understand the relationships between the preservation of the palaeomagnetic record and the succession of deformation events recorded in the Caledonian basement of Western Svalbard, further studies are required.

**Author Contributions:** M.B. collected and prepared the samples, performed the experiments, analysed and interpreted the data, prepared figures and tables, wrote the paper; K.M. helped in the interpretation of the data, contributed to the preparation part of the paper related to palaeomagnetic investigation and critically reviewed the manuscript; G.M. helped in the interpretation of structural geology data, helped write the geological setting and reviewed in detail the final version of the manuscript; K.N. supported the mineralogical and petrographic interpretations.

**Funding:** This study is part of the PALMAG project 2012–2016: Integration of palaeomagnetic, isotopic and structural data to understand Svalbard Caledonian Terranes assemblage funded by Polish National Science Centre (NSC)—grant number 2011/03/D/ST10/05193. This research is also partially financed from the funds of the Leading National Research Centre (KNOW) (03/KNOW2/2014) received by the Centre for Polar Studies for the period 2014–2018 and partially supported by statutory activities No. 3841/E-41/S/2017 of the Ministry of Science and Higher Education of Poland.

**Acknowledgments:** We would like to thank to Katarzyna Dudzisz for help during field work and to Aleksandra Hołda-Michalska for her time devoted to graphical revision.

**Conflicts of Interest:** The authors declare no conflict of interest.

## Appendix A. Anisotropy of Magnetic Susceptibility

All meta-igneous sites are characterized by moderate values of the bulk magnetic susceptibility ( $K_m$ ) in the range between  $\sim 7.0 \times 10^{-4}$  up to  $\sim 1.9 \times 10^{-3}$  SI (Figure A1A). The corrected anisotropy degree ( $P_j$ ) *sensu* Jelinek [65], in the majority of samples, does not exceed 4–5% but may occasionally reach 8%. The exception is in sites from DAUST5 where distinct samples reveal higher values of  $P_j$  within the range 10–20% (Figure A1B). Metadolerite sites from Daudmannsdalen (DAUST1–4) are characterized by an oblate shape of the AMS ellipsoid ( $T > 0$ ) (Figure A1C) with a precisely defined AMS foliation (K1/K2 plane). It should be noted that all four sites from Daudmannsdalen show a stable trend of the AMS foliation  $10^\circ$ – $30^\circ$  east of north and a dip  $40^\circ$ – $70^\circ$  to NW. Metadolerites from Daudmannsøyra near the shore site (DAUST5) and Protectorbreen (PROST6) reveal a composite oblate-prolate pattern of AMS. A Tri-axial pattern of the AMS is observed in sites DAUST3, DAUST4 and PROST6.

There are two main structural features which can be traced in the majority of the investigated sites. The first are relicts of the bedding of the host metacarbonates, parallel to the metacarbonate-dolerite contact. The bedding of the host metacarbonates varies from a strike and dip 060/20 N for Daudmannsdalen (the average for sites DAUST1–4), 130/10 N for Daudmannsøyra (DAUST5) and 095/30 S for Protectorbreen (PROST6). In sites DAUST1–4 (Daudmannsdalen) it was also possible to measure the cleavage with an average strike and dip of 070/60 N. It is evident, however, that the AMS foliations (K1/K3 planes) in all of the sites are oblique to both bedding and cleavage surfaces (if measurable Figure A1D). The observed AMS ellipsoids can reflect a summary of the effects of different fabric elements related to structural stages of rock evolution [66]. The maximum axes of AMS (K1) are oblique to the identified NRM components.

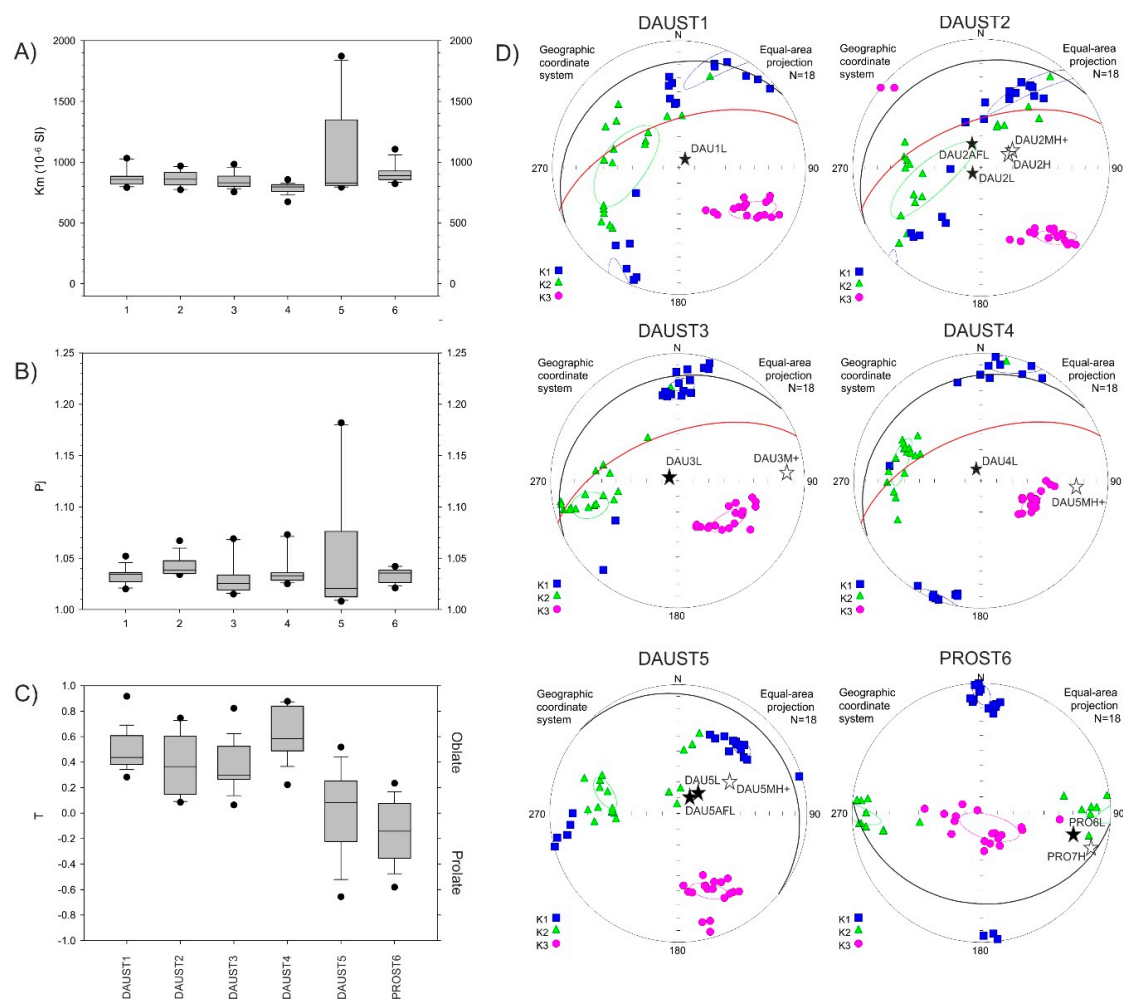


**Figure A1.** The results of anisotropy of magnetic susceptibility (AMS) experiments of metadolerites and metacarbonates rocks from SW Oscar II Land; (A) diagram of the mean magnetic susceptibility (Km); (B) diagram of corrected anisotropy degree ( $P_i$ ) sensu Jelinek [65] (C) diagram of the shape parameter ( $T$ ); grey boxes—25% and 75% percentiles; horizontal lines inside boxes—the mean values; black dots—maximum and minimum values; vertical lines (whiskers)—10% and 90% percentiles (D) Equal-area projections of principal susceptibility axes; points K1, K2, K3 represents maximum, intermediate and minimum axes respectively with  $\alpha_{95}$  confidence ellipses for each population. Lower-hemisphere—filled symbols; upper hemisphere—open symbol. Orientations of all calculated palaeomagnetic components are marked by stars. The parameters of the host metacarbonates bedding and cleavage are marked by black and red arcs respectively.

## References

1. Harland, W.B.; Wright, N. Alternative hypothesis for the pre-Carboniferous evolution of Svalbard. *Norsk Polarinst. Skr.* **1979**, *167*, 89–117.
2. Gee, D.G. Svalbard's Caledonian terranes reviewed. *Geol. Foeren. Stockholm Forh.* **1986**, *108*, 284–286. [[CrossRef](#)]
3. Gee, D.G.; Page, L.M. Caledonian Terrane Assembly on Svalbard: New Evidence from Ar/Ar Dating in Ny Friesland. *Am. J. Sci.* **1994**, *294*, 1166–1186. [[CrossRef](#)]
4. Gee, D.G.; Tebenkov, A.M. Svalbard: A fragment of the Laurentian margin. In *The Neoproterozoic Timanide Orogen of Eastern Baltica*; Gee, D.G., Pease, V., Eds.; The Geological Society of London: London, UK, 2004; Volume 30, pp. 191–206.

5. Kościńska, K.; Majka, J.; Mazur, S.; Krumbholz, M.; Klonowska, I.; Manecki, M.; Czerny, J.; Dwornik, M. Blueschist facies metamorphism in Nordenskiöld Land of west-central Svalbard. *Terra Nova* **2014**, *26*, 377–386. [[CrossRef](#)]
6. Mazur, S.; Czerny, J.; Majka, J.; Manecki, M.; Holm, D.K.; Smyrak, A.; Wypych, A. A strike-slip terrane boundary in Wedel Jarlsberg Land, Svalbard, and its bearing on correlations of SW Spitsbergen with the Pearya terrane and Timanide belt. *J. Geol. Soc.* **2009**, *166*, 529–544. [[CrossRef](#)]
7. Majka, J.; Kościńska, K.; Mazur, S.; Czerny, J.; Piepjohn, K.; Dwornik, M.; Manecki, M. Two garnet growth events in polymetamorphic rocks in southwest Spitsbergen, Norway: Insight in the history of Neoproterozoic and early Paleozoic metamorphism in the High Arctic. *Can. J. Earth Sci.* **2015**, *52*, 1–17. [[CrossRef](#)]
8. Majka, J.; Kościńska, K. Magmatic and metamorphic events recorded within the Southwestern Basement Province of Svalbard. *Arktos* **2017**, *3*, 5. [[CrossRef](#)]
9. Piepjohn, K.; von Gosen, W.; Tessensohn, F.; Reinhardt, L.; McClelland, W.C.; Dallmann, W.K.; Gaedicke, C.; Harrison, J.C. Tectonic map of the Ellesmerian and Eurekan deformation belts on Svalbard, North Greenland, and the Queen Elizabeth Islands (Canadian Arctic). *Arktos* **2015**, *1*, 12. [[CrossRef](#)]
10. Dallmann, W.K.; Elvevold, S.; Majka, J.; Piepjohn, K. Chapter 8: Tectonics and tectonothermal events. In *Geoscience Atlas of Svalbard*; Dallmann, W.K., Ed.; Norsk Polarinstitut: Tromsø, Norway, 2015; Volume 148, pp. 175–220.
11. Gasser, D.; Andresen, A. Caledonian terrane amalgamation of Svalbard: Detrital zircon provenance of Mesoproterozoic to Carboniferous strata from Oscar II Land, western Spitsbergen. *Geol. Mag.* **2013**, *150*, 1103–1126. [[CrossRef](#)]
12. Michalski, K.; Lewandowski, M.; Manby, G.M. New palaeomagnetic, petrographic and  $^{40}\text{Ar}/^{39}\text{Ar}$  data to test palaeogeographic reconstructions of Caledonide Svalbard. *Geol. Mag.* **2012**, *149*, 696–721. [[CrossRef](#)]
13. Michalski, K.; Nejbort, K.; Domańska-Siuda, J.; Manby, G. New palaeomagnetic data from metamorphosed carbonates of Western Spitsbergen, Oscar II Land. *Pol. Polar Res.* **2014**, *35*, 553–592. [[CrossRef](#)]
14. Michalski, K.; Manby, G.; Nejbort, K.; Domańska-Siuda, J.; Burzyński, M. Using palaeomagnetic and isotopic data to investigate late to post-Caledonian tectonothermal processes within the Western Terrane of Svalbard. *J. Geol. Soc. Lond.* **2017**, *174*, 572. [[CrossRef](#)]
15. Burzyński, M.; Michalski, K.; Nejbort, K.; Domańska-Siuda, J.; Manby, G. High resolution mineralogical and rock magnetic study of ferromagnetic phases in metabasites from Oscar II Land, Western Spitsbergen—Towards reliable model linking mineralogical and palaeomagnetic data. *Geophys. J. Int.* **2017**, *210*, 390–405. [[CrossRef](#)]
16. Trettin, H.P. Pearya: A composite terrane with Caledonian affinities in northern Ellesmere Island. *Can. J. Earth Sci.* **1987**, *24*, 224–245. [[CrossRef](#)]
17. Piepjohn, K. The Svalbardian-Ellesmerian deformation of the Old Red Sandstone and the pore-Devonian basement in NW Spitsbergen (Svalbard). In *New Perspectives on the Old Red Sandstone*; Friend, P.F., Williams, B.P.J., Eds.; Special Publications; Geological Society of London: London, UK, 2000; Volume 180, pp. 585–601.
18. Kościńska, K.; Majka, J. A review of magmatic and metamorphic events recorded by crystalline basement of Southwestern Svalbard. In Proceedings of the 33rd Nordic Geological Winter Meeting, Denmark, Copenhagen, 10–12 January 2018.
19. Majka, J.; Mazur, S.; Manecki, M.; Czerny, J.; Holm, D.K. Late Neoproterozoic amphibolite-facies metamorphism of a pre-Caledonian basement block in southwest Wedel Jarlsberg Land, Spitsbergen: New evidence from U–Th–Pb dating of monazite. *Geol. Mag.* **2008**, *145*, 822–830. [[CrossRef](#)]
20. Majka, J.; Czerny, J.; Mazur, S.; Holm, D.K.; Manecki, M. Neoproterozoic metamorphic evolution of the Isbjørnhamna Group rocks from south-western Svalbard. *Polar Res.* **2010**, *29*, 250–264.
21. Majka, J.; Be'eri-Shlevins, Y.; Gee, D.G.; Czerny, J.; Frei, D.; Ladenberger, A. Torellian (c. 640 Ma) metamorphic overprint of Tonian (c. 950 Ma) basement in the Caledonides of southwestern Svalbard. *Geol. Mag.* **2014**, *151*, 732–748. [[CrossRef](#)]
22. Birkenmajer, K. Caledonides of Svalbard and plate tectonics. *Bull. Geol. Soc. Den.* **1975**, *24*, 1–19.
23. Bjørnerud, M. Upper Proterozoic unconformity in northern Wedel-Jarlsberg Land, southwest Spitsbergen: Lithostratigraphy and tectonic implications. *Polar Res.* **1990**, *8*, 127–140. [[CrossRef](#)]
24. Ohta, Y. Geochemistry of Precambrian basic igneous rocks between St Jonsfjorden and Isfjorden, central western Spitsbergen, Svalbard. *Polar Res.* **1985**, *3*, 49–67. [[CrossRef](#)]

25. Czerny, J. *Petrogenesis of Metavolcanites of the Southern Part of Wedel Jarlsberg Land (Spitsbergen)*; Wydawnictwo Oddziału PAN: Kraków, Poland, 1999; pp. 1–88.
26. Harland, W.B. *The Geology of Svalbard*; Geological Society of London: London, UK, 1997; Volume 17, p. 521. [[CrossRef](#)]
27. Dallmeyer, R.D.; Peucat, J.J.; Hirajima, T.; Ohta, Y. Tectonothermal chronology within a blueschist-eclogite complex, west-central Spitsbergen, Svalbard: Evidence from  $^{40}\text{Ar}/^{39}\text{Ar}$  and Rb/Sr mineral ages. *Lithos* **1990**, *24*, 291–304. [[CrossRef](#)]
28. Lyberis, N.; Manby, G.M. The origin of the West Spitsbergen Fold Belt from geological constraints and plate kinematics: Implications for the Arctic. *Tectonophysics* **1993**, *224*, 371–391. [[CrossRef](#)]
29. Piepjohn, K.; von Gosen, W.; Tessensohn, F. The Eurekan deformation in the Arctic: An outline. *J. Geol. Soc.* **2016**, *173*, 1007. [[CrossRef](#)]
30. Harland, W.B.; Horsfield, W.T.; Manby, G.M.; Morris, A.P. An outline pre-Carboniferous stratigraphy of West Spitsbergen. *Norsk Polarinst. Skr.* **1979**, *167*, 119–140.
31. Bergh, S.G.; Ohta, Y.; Andresen, A.; Maher, H.D.; Braathen, A.; Dallmann, W.K. *St. Jonsfjorden, Svalbard, 1:100,000*; Theme Map No. 34; Norsk Polarinstitutt: Tromsø, Norway, 2003.
32. Hjelle, A.; Ohta, Y.; Wisnes, T. Hecla Hoek rocks of Oscar II Land and Prins Karls Forland. *Norsk Polarinst. Skr.* **1979**, *167*, 145–170.
33. Kanat, L.; Morris, A. *A Working Hypothesis for Central Western Oscar II Land, Spitsbergen*; Skrifter NR. 190; Norsk Polarinstitutt: Tromsø, Norway, 1988.
34. Ohta, Y.; Hjelle, A.; Andresen, A.; Dallmann, W.K.; Salvigsen, O. *Isfjorden, Svalbard 1:100,000*; Theme Map No. 16; Norsk Polarinstitutt: Tromsø, Norway, 1992.
35. Ohta, Y.; Hjelle, A.; Andresen, A.; Dallmann, W.K.; Sålvisgen, O. *Geological Map of Svalbard, 1:100,000*; Sheet B9G Isfjorden, with Description; Norsk Polarinstitutt: Tromsø, Norway, 1991; Temakart, 16.
36. Maher, D.M., Jr.; Bergh, S.; Braathen, A.; Ohta, Y. Svartfjella, Eidembukta, and Daudmannsodden lineament: Tertiary orogen-parallel motion in the crystalline hinterland of Spitsbergen's fold-thrust belt. *Tectonics* **1997**, *16*, 88–106. [[CrossRef](#)]
37. Tessensohn, F.; Von Gosen, W.; Piepjohn, K. Permo-Carboniferous slivers infolded in the basement of Western Oscar II Land. *Geol. Jahrbuch* **2001**, *B91*, 161–199.
38. Hjelle, A.; Piepjohn, K.; Saalmann, K.; Ohta, Y.; Salvigsen, O.; Thieding, F.; Dallmann, W.K. *Kongsfjorden, Svalbard, 1:100,000*; Theme Map No. 30; Norsk Polarinstitutt: Tromsø, Norway, 1999.
39. McAndrew, J. Calibration of a Frantz isodynamic separator and its application to mineral separation. *Proc. Aust. Inst. Min. Met.* **1957**, *181*, 59–73.
40. Rosenblum, S.; Brownfield, I.K. *Magnetic Susceptibilities of Minerals*; US Geological Survey Open-File Report 99-529; US Department of the Interior: Washington, DC, USA, 2000. Available online: <http://pubs.usgs.gov/of/1999/ofr-99-0529/> (accessed on 28 June 2018).
41. Lowrie, W. Identification of ferromagnetic minerals in a rock by coercivity and unblocking temperature properties. *Geophys. Res. Lett.* **1990**, *17*, 159–162. [[CrossRef](#)]
42. Chadima, M.; Jelinek, V. Anisoft 4.2. Anisotropy Data Browser. AGICO, 2009. Available online: <http://www.agico.com/> (accessed on 28 June 2018).
43. Chadima, M.; Hrouda, F. Remasoft 3.0 Paleomagnetic Data Browser and Analyzer. AGICO, 2009. Available online: <http://www.agico.com/> (accessed on 28 June 2018).
44. Kirschvink, J.L. The least-squares line and plane and the analysis of palaeomagnetic data. *Geophys. J. Int.* **1980**, *62*, 699–718. [[CrossRef](#)]
45. Fisher, R. Dispersion on a sphere. *Proc. R. Soc. Lond. Ser. A* **1953**, *217*, 295–305. [[CrossRef](#)]
46. Butler, R.F. *Paleomagnetism: Magnetic Domains to Geological Terranes*; Blackwell Scientific: Boston, MA, USA, 1992.
47. Van der Voo, R. *Paleomagnetism of the Atlantic, Tethys and Iapetus Oceans*; Cambridge University Press: Cambridge, UK, 1993.
48. Torsvik, T.H.; van der Voo, R.; Preeden, U.; Mac Niocaill, C.; Steinberger, B.; Doubrovine, P.V.; van Hinsbergen, D.J.J.; Domeier, M.; Gaina, C.; Tohver, E.; et al. Phanerozoic polar wander, paleogeography and dynamics. *Earth-Sci. Rev.* **2012**, *114*, 325–368. [[CrossRef](#)]

49. Michalski, K. Palaeomagnetism of metacarbonates and fracture fills of Kongsfjorden islands (western Spitsbergen): Towards a better understanding of late- to post-Caledonian tectonic rotations. *Pol. Polar Res.* **2018**, *39*, 51–75. [[CrossRef](#)]
50. Szlachta, K.; Michalski, K.; Brzózka, K.; Górka, B.; Gałazka-Friedman, J. Comparison of magnetic and Mössbauer results obtained for Palaeozoic rocks of Hornsund, Southern Spitsbergen, Arctic. *Acta Phys. Pol. A* **2008**, *114*, 1675–1682. [[CrossRef](#)]
51. Frost, B.R. Magnetic petrology: Factors that control the occurrence of magnetite in crustal rocks. In *Oxide Minerals: Petrologic and Magnetic Significance*; Lindsley, D.H., Ed.; Mineralogical Society of America: Chantilly, VA, USA, 1991; Volume 25, pp. 489–509.
52. Frost, B.R.; Lindsley, D.H. Occurrence of iron–titanium oxides in igneous rocks. In *Oxide Minerals: Petrologic and Magnetic Significance*; Lindsley, D.H., Ed.; Mineralogical Society of America: Chantilly, VA, USA, 1991; Volume 25, pp. 433–468.
53. Haggerty, S.E. *Opaque Mineral Oxides in Terrestrial Igneous Rocks*; Mineralogical Society of America: Chantilly, VA, USA, 1976; Volume 3, pp. 101–300.
54. Haggerty, S.E. Oxide textures—A mini-atlas. In *Oxide Minerals: Petrologic and Magnetic Significance*; Lindsley, D.H., Ed.; Mineralogical Society of America: Chantilly, VA, USA, 1991; Volume 25, pp. 129–219.
55. Harlov, D.; Tropper, P.; Seifert, W.; Nijland, T.; Förster, H.J. Formation of Al-rich titanite (CaTiSiO<sub>4</sub>O–CaAlSiO<sub>4</sub>OH) reaction rims on ilmenite in metamorphic rocks as a function of  $f\text{H}_2\text{O}$  and  $f\text{O}_2$ . *Lithos* **2006**, *88*, 72–84. [[CrossRef](#)]
56. Xirouchakis, D.; Lindsley, D.H. Equilibria among titanite, hedenbergite, fayalite, quartz, ilmenite and magnetite: Experiments and internally consistent thermodynamic data for titanite. *Am. Mineral.* **1998**, *83*, 712–725. [[CrossRef](#)]
57. Hopkinson, J. Magnetic and other Physical Properties of Iron at a High Temperature. *Philos. Trans. R. Soc. Lond.* **1889**, *A180*, 443–465. [[CrossRef](#)]
58. Hrouda, F. A technique for the measurement of thermal changes of magnetic susceptibility of weakly magnetic rocks by the CS-2 apparatus and KLY-2 Kappabridge. *Geophys. J. Int.* **1994**, *118*, 604–612. [[CrossRef](#)]
59. Li, Z.W.; Dobson, J.; Chen, Z.; Chang, W.J.; St. Pierre, T.G. Multimodal investigation of thermally induced changes in magnetic fabric and magnetic mineralogy. *Geophys. J. Int.* **2003**, *135*, 988–998. [[CrossRef](#)]
60. Özdemir, Ö. Inversion of titanomagemites. *Phys. Earth Planet. Inter.* **1987**, *46*, 184–196. [[CrossRef](#)]
61. Matzka, J.; Krása, D. Oceanic basalt continuous thermal demagnetization curves. *Geophys. J. Int.* **2007**, *169*, 941–950. [[CrossRef](#)]
62. Dekkers, M.J. Magnetic properties of natural pyrrhotite part 1: Behavior of initial susceptibility and saturation-magnetization related parameters in a grain-size dependent framework. *Phys. Earth Planet. Inter.* **1988**, *52*, 376–393. [[CrossRef](#)]
63. Dunlop, D.J.; Özdemir, Ö. *Rock Magnetism Fundamentals and Frontiers*; Cambridge University Press: Cambridge, UK, 1997.
64. Clark, S.A.; Glorstad-Clark, E.; Faleide, J.I.; Schmid, D.; Hartz, E.H.; Fjeldskaar, W. Southwest Barents Sea rift basin evolution: Comparing results from backstripping and time forward modelling. *Basin Res.* **2014**, *26*, 550–566. [[CrossRef](#)]
65. Jelinek, V. Characterization of the magnetic fabrics of rocks. *Tectonophysics* **1981**, *79*, 63–67. [[CrossRef](#)]
66. Oliva-Urcia, B.; Román-Berdiel, T.; Casas, A.M.; Pueyo, E.L.; Osácar, C. Tertiary compressional overprint on Aptian–Albian extensional magnetic fabrics, North-Pyrenean Zone. *J. Struct. Geol.* **2010**, *32*, 362–376. [[CrossRef](#)]

